1997 CEDAR Workshop
Boulder, Colorado
June 8-13, 1997

Tutorial Lecture

by Roger Smith
University of Alaska

The Observation and Interpretation of Vertical Winds in the Mesosphere and Thermosphere

VERTICAL WINDS

- Motivation: Vertical winds put the "barbie source" on the atmospheric "steak".
- Basic considerations and examination of global vertical winds
- Small scale vertical winds and examination of strong events
- Summary

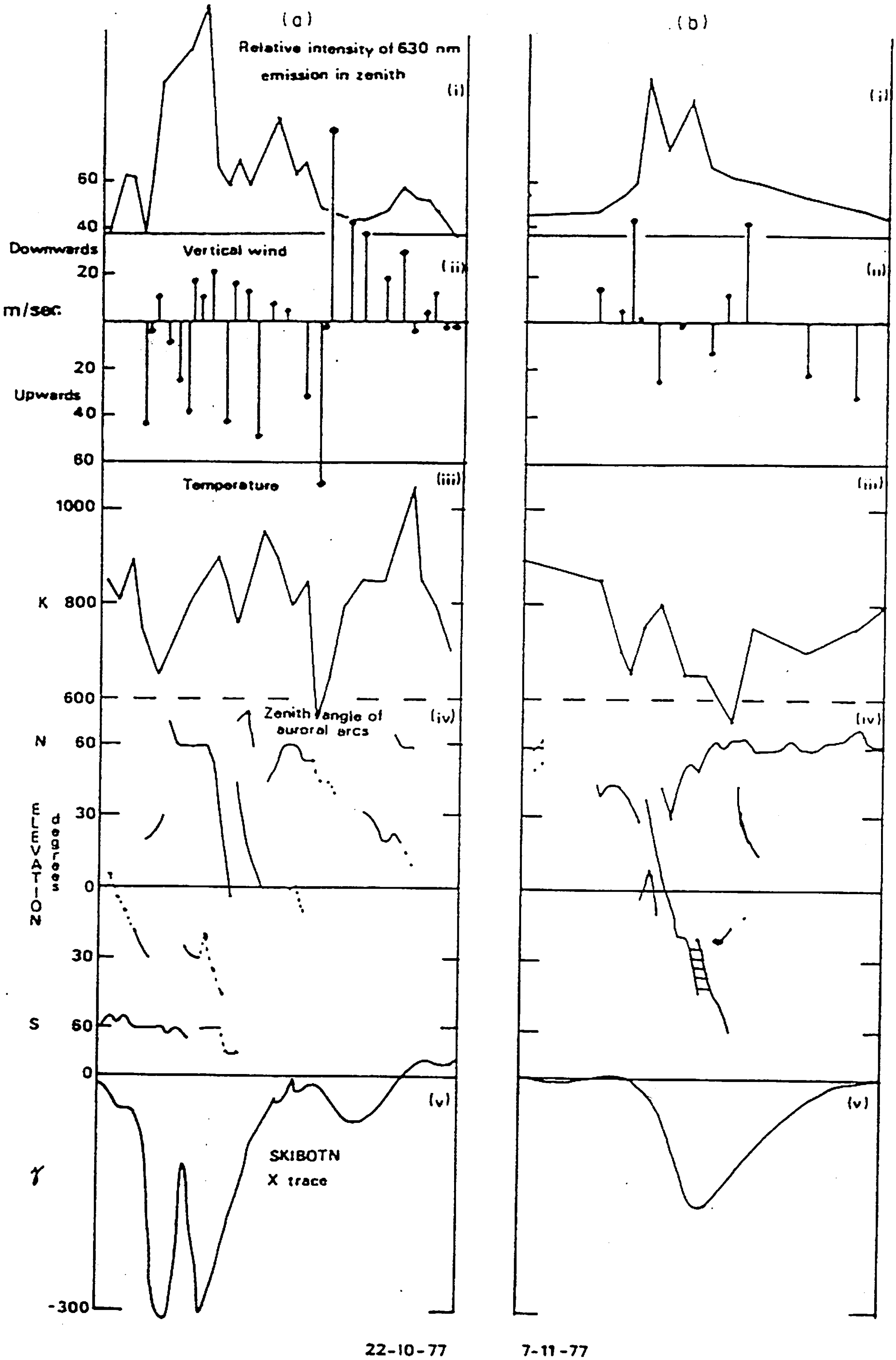

FIG. 1. DATA FROM SKIBOTN, 1977.
Panel (a) shows a compilation of measurements made between 21.00 and 01.00 U.T. on the night of 22/23 October. Panel (b) shows a similar compilation for 20.00–24.00 U.T. on 7 November. Subsections (i)–(v) of each panel are on the same time axis, and show, respectively, the zenith intensity at 630 nm, the vertical component of thermospheric wind, the thermospheric temperature at the height of the wind measurement, the meridional elevation of auroral arcs at 630 nm and the X-component of the local magnetogram.

SMOKING GUN (1)

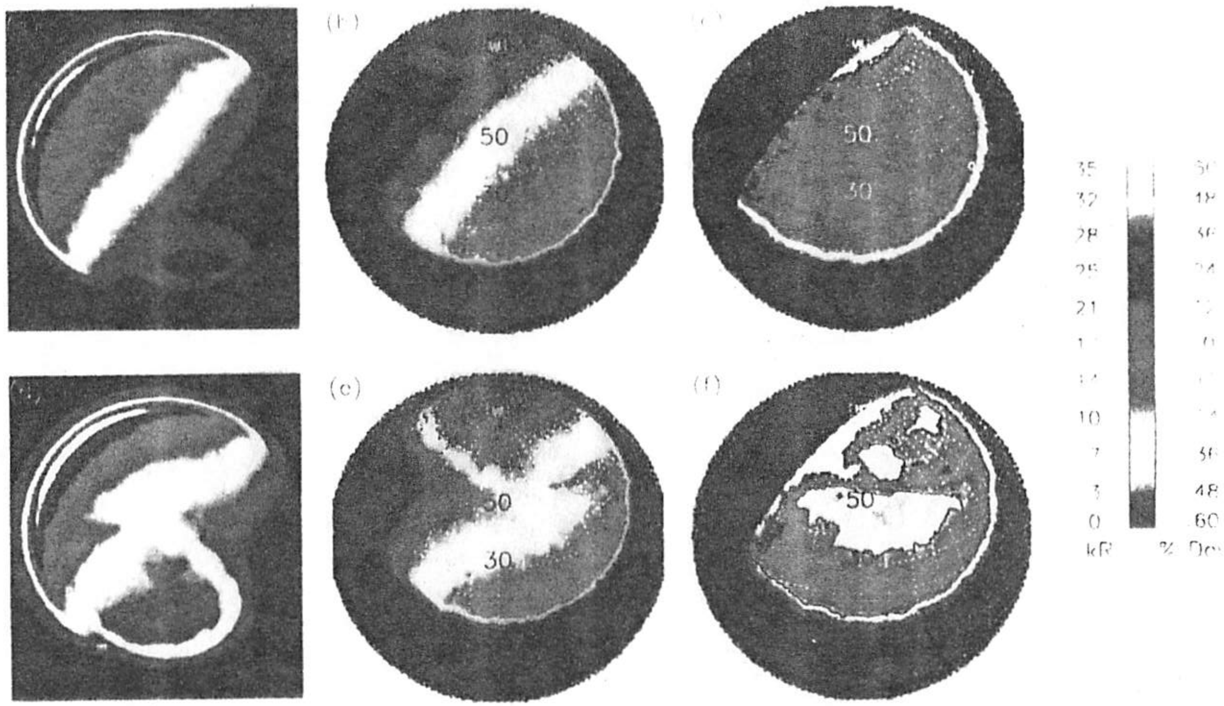

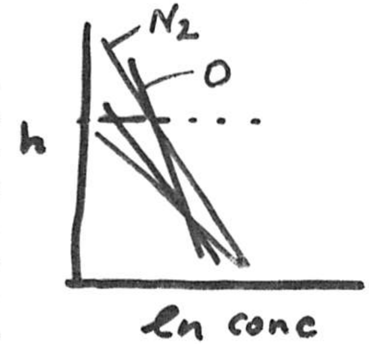

Figure 1. DE-1 images of Earth at FUV wavelengths 123-160 nm. (a) Original image on 31 October 1981 at 0629 UT. Sun is towards upper left. (b) Partial image mapped onto an orthographic projection as viewed in the morning sector at geographic 40°N, 30°W, (~0830 LST). A geographic coordinate grid is overlaid, and latitudes are labeled at the CML. Diameter of Earth is increased by ~40%. (c) Percent deviation of brightness in Figure 1b as compared to reference values. (d) Original image on 22 October 1981 at 1709 UT (40°N, 230°E, ~0830 LST). The auroral oval is visible towards the bottom on this magnetically active day. (e) Figure 1d mapped using the format of Figure 1b. (f) Percent deviation of brightness in Figure 1e. FUV brightness is coded in kR using values to the left of the color bar. Percent deviation is given to the right

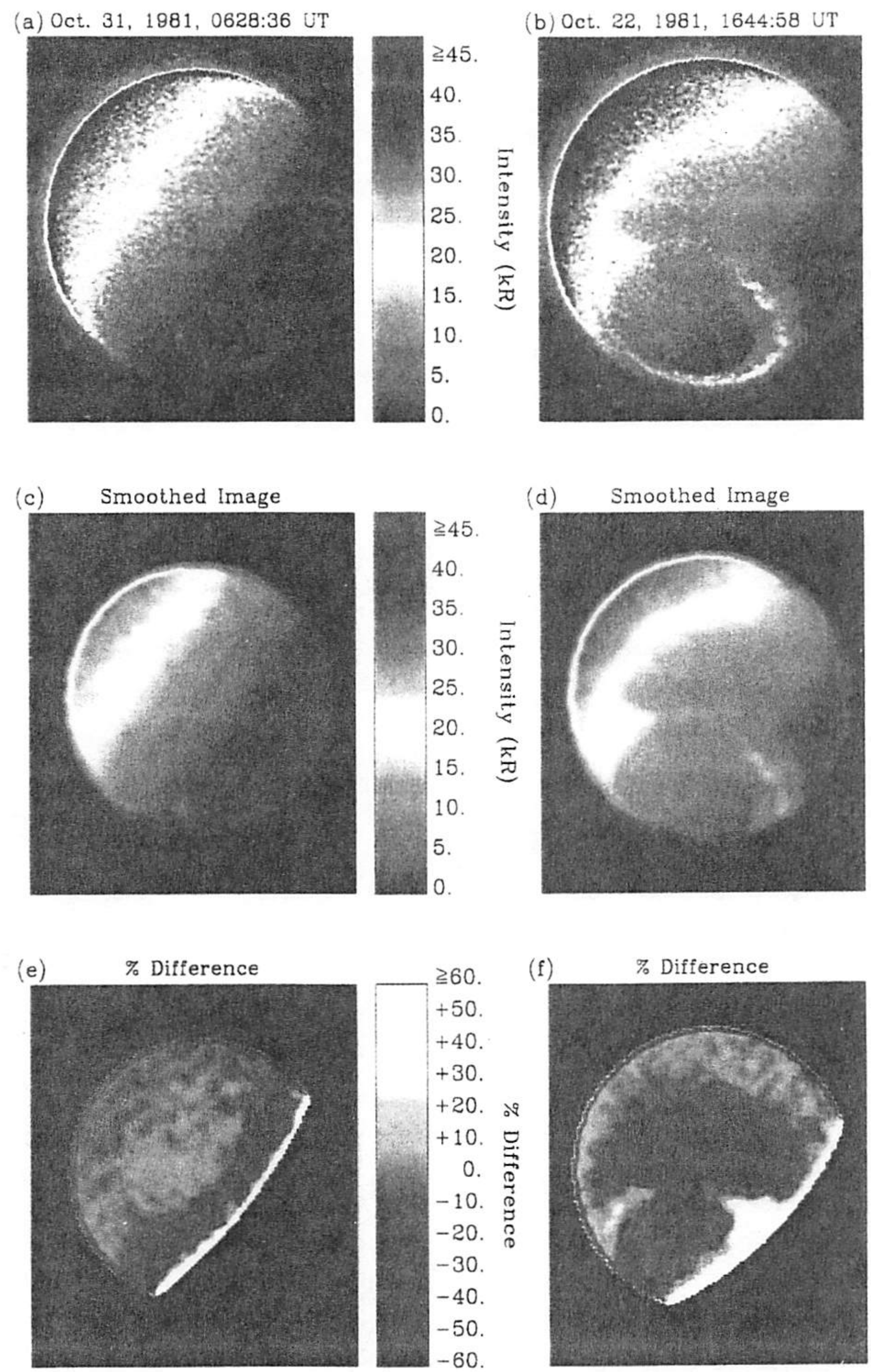

Plate 1. (a) FUV image of Earth obtained with the DE 1 satellite beginning at 0628:36 UT on October 31 (day 304), 1981. This image at wavelengths 123–165 nm is from a period of low geomagnetic activity in which *AE* remained <100 nT for more than four hours prior to imaging. The image is presented in satellite coordinates, with the orbit plane vertically bisecting the image, the Sun toward the top left, and the weak signature of the northern auroral oval at the bottom right near the limb. Note the smooth variations in FUV brightness across the image in the sunlit hemisphere. (b) The DE 1 image obtained at 1644:58 UT on October 22 (day 295), 1981, after a period of intense magnetic activity (*AE* ~1500 nT). The auroral oval is large and prominent, with a substantial decrease in brightness of the dayglow in the morning sector at subauroral latitudes. The satellite altitude and local solar time are nearly identical to those for the image in Plate 1a. These two images are in the original, unprocessed format. Broadband brightness, in kilorayleighs (kR), is specified by the color bar. (c) The image of Plate 1a after smoothing and removal of the limb region, as discussed in the text. (d) The image of Plate 1b after smoothing and removal of the limb region, using the format of Plate 1c. (e) The percent difference between the original image in Plate 1a and the reference (model) image. The algorithm for the pixel-by-pixel computation is ((image-model)/model), and the color bar for conversion to percent difference is presented between panels e and f. (f) The percent difference between the original image in Plate 1b and the reference (model) image, in the format of Plate 1e.

SMOKING GUN (2)

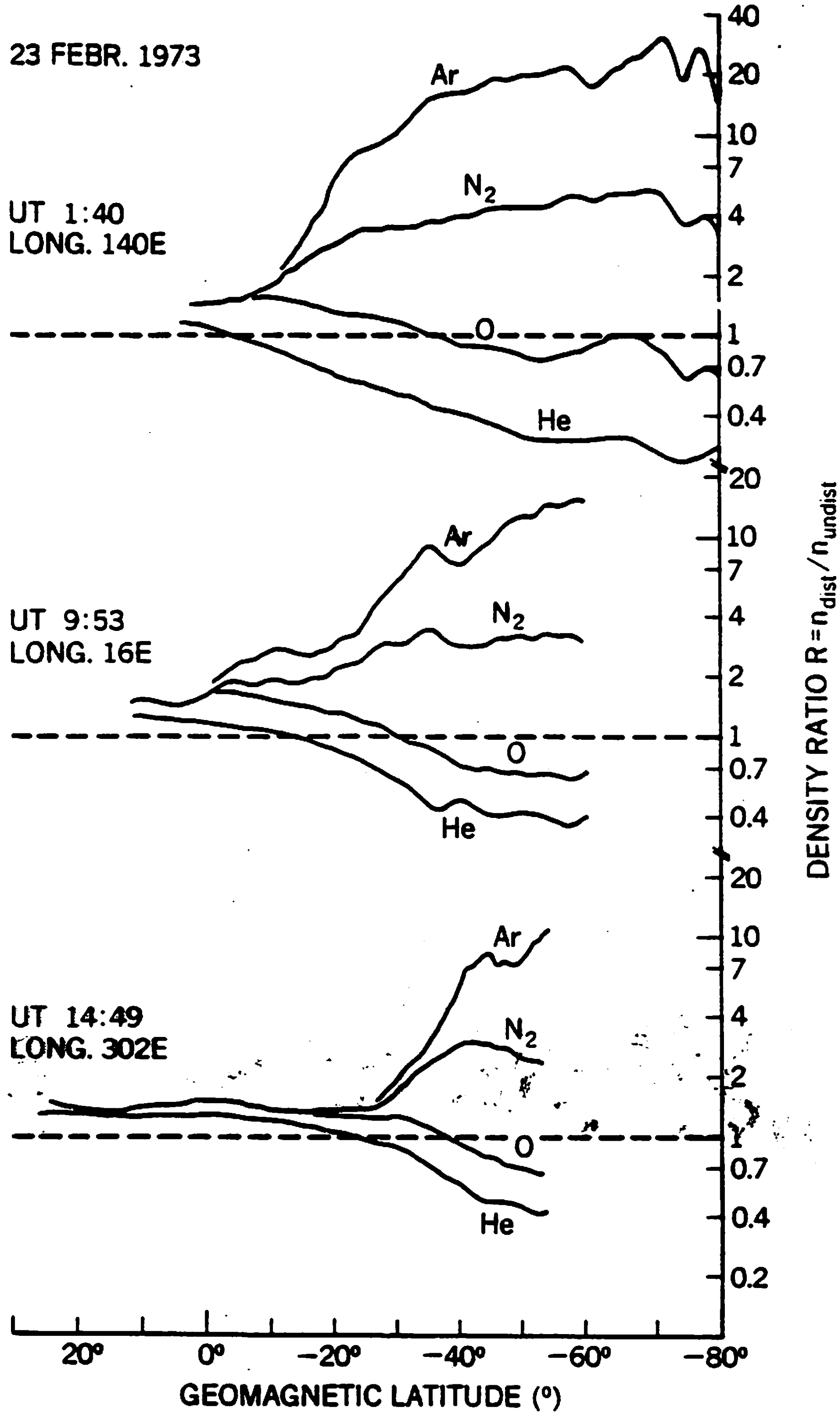

Figure 8. Composition measurements from the gas analyzer on ESRO-4 (Trinks et al., 1975) during the magnetic storm of February 23, 1973.

COMMENTS ON NATE + WATS

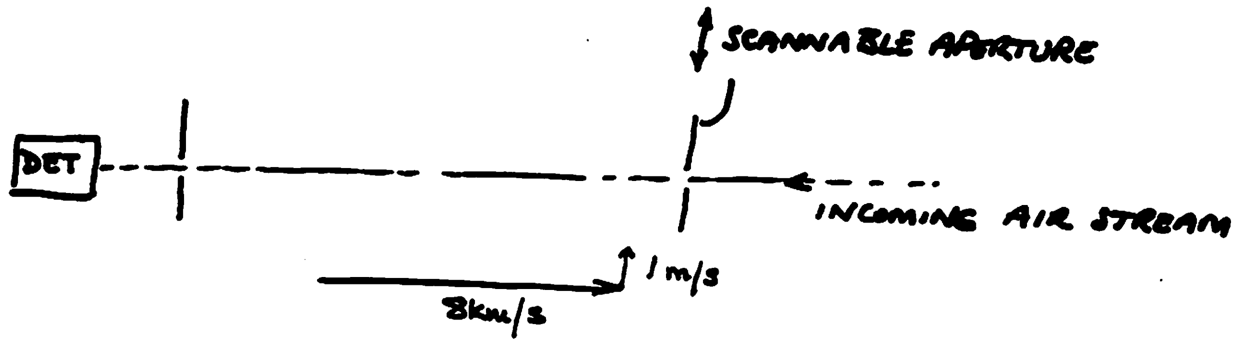

1. Accurate knowledge of spacecraft orientation is critical

COMMENTS ON FPI OBSERVATIONS

1. FREQUENCY CALIBRATION

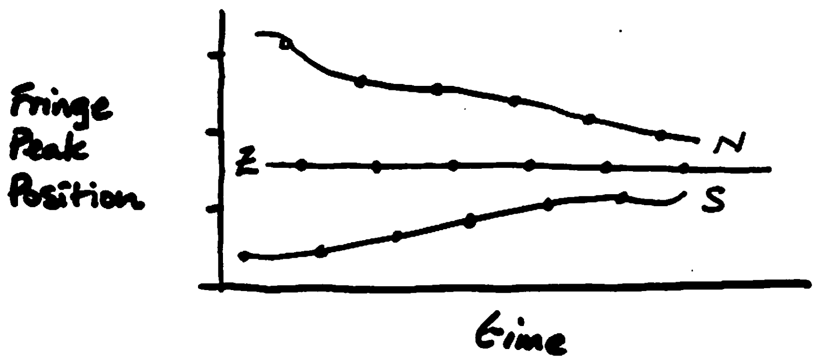

At 630nm, no lab source for calibration

∴ Use mean zenith position.

if wrong then vertical wind implied and also horizontal divergence.

2. FREQUENCY STABILITY

PHASE LOCKED in operation or TRACKED for post hoc lock.

< 3m/s

3. LINE OF SIGHT SAMPLING OF VECTOR FIELD

a. instrument only senses divergence

b. Vertical wind is only observation which is unambiguous

c. but only know vertical wind in one place — hence must insert assumption to infer horizontal components.

d. no information on vortical flow (ie no curl, only div) must insert assumption to infer cross-LOS components.

e. horizontal wind fields reconstructed from LOS data may have artifacts due to erroneous assumptions in (c) & (d).

Spencer et al., 1976

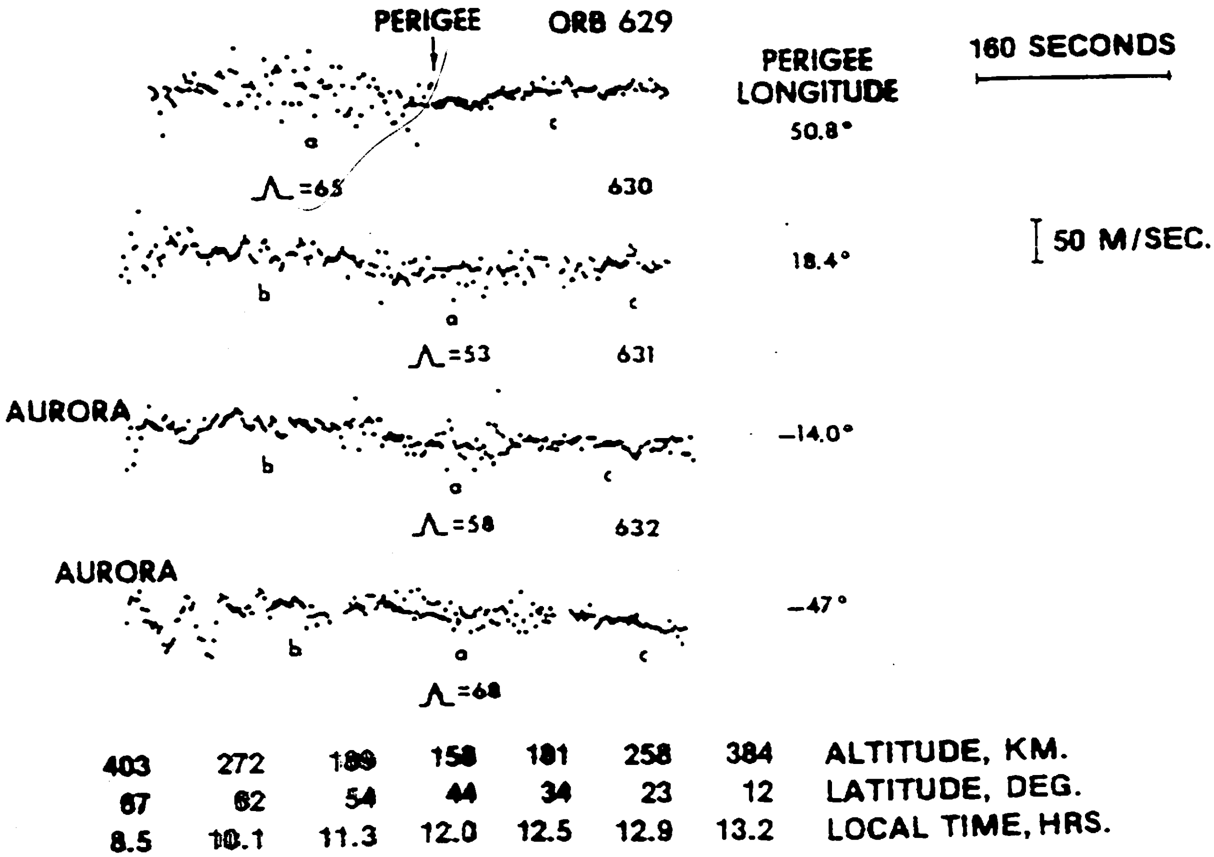

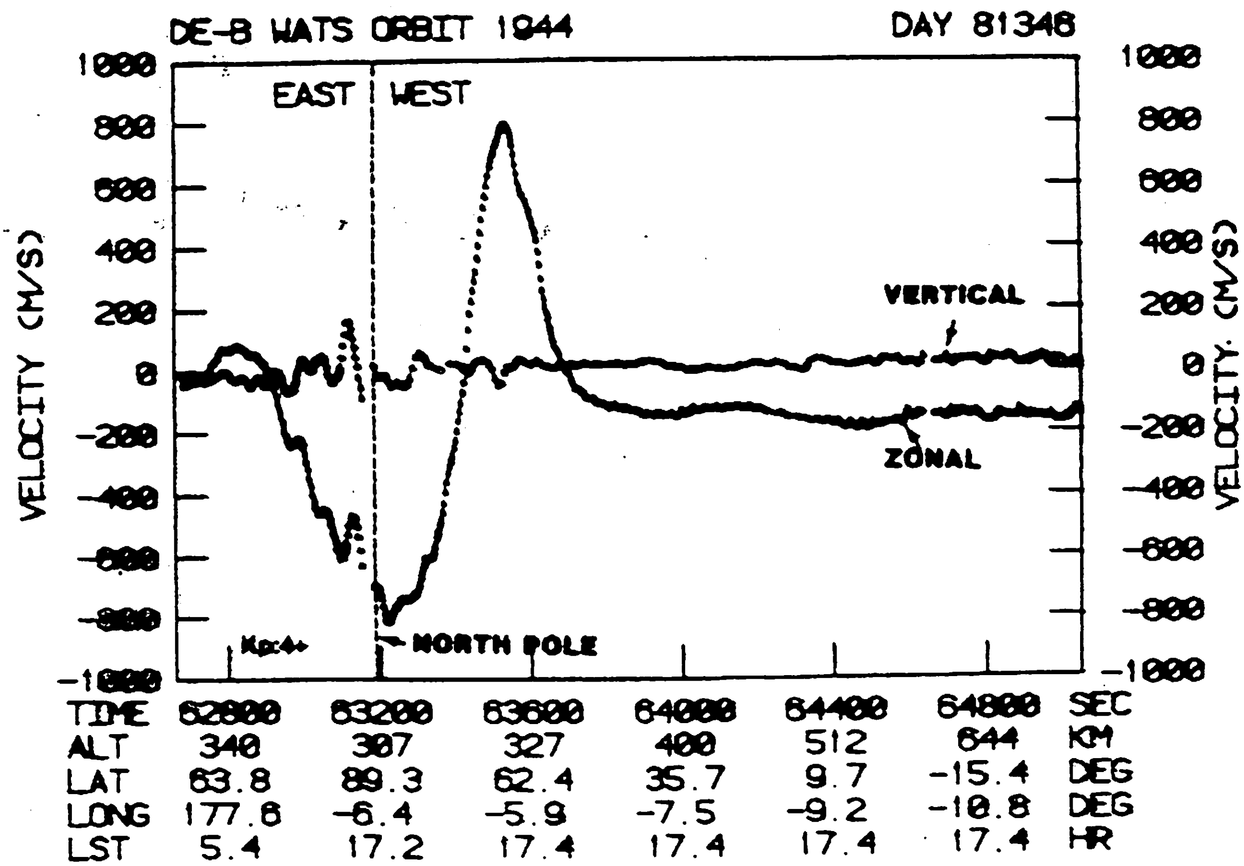

Fig. 1. Example of north pole zonal and vertical components of neutral particle winds from the DE-2 WATS instrument. Sign convention: westward winds are positive after spacecraft passes the north pole.

Spencer et al
1982

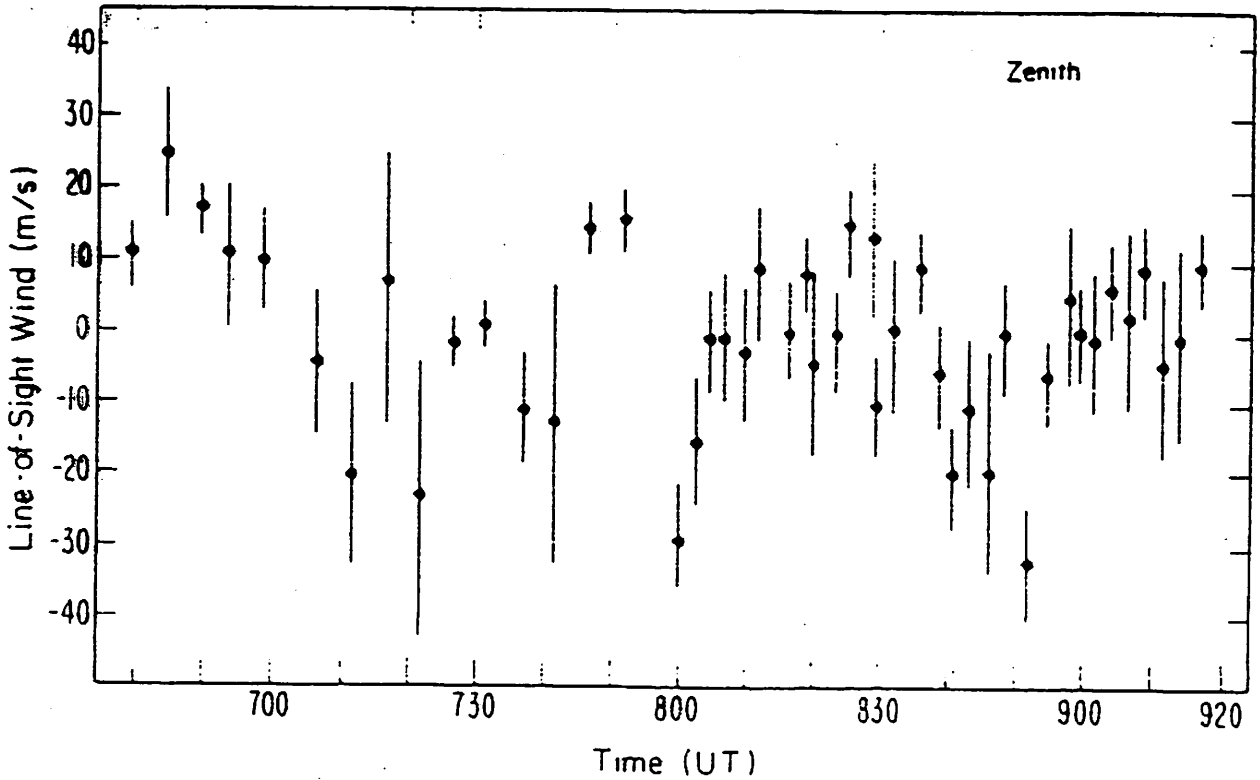

Fig. 3. Combined vertical motions of Figures 1 and 2.

Hernandez
1982

Siplr et al., 1995

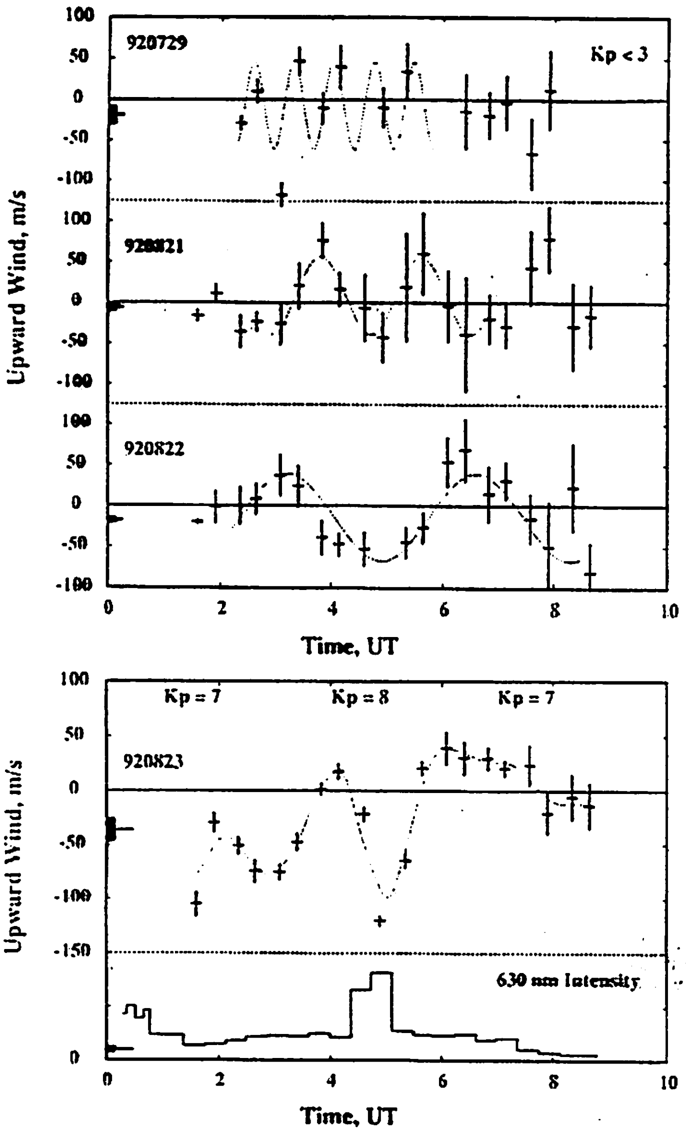

Fig. 4. (a) Vertical winds derived from bistatic measurements on three geomagnetically quiet nights, 29 July, 21 and 22 August 1992. The vertical bars show the uncertainty in the derived winds, and the horizontal bars represent the approximate time interval for the measurements. The light dotted lines represent constant-amplitude waves which have been fitted to the data. (b) Vertical winds during a disturbed period on the night of 1992 August 23. In this case, the light dotted line represents the data after being smoothed with a 1.2 h time constant. The (uncalibrated) 630 nm intensity for the

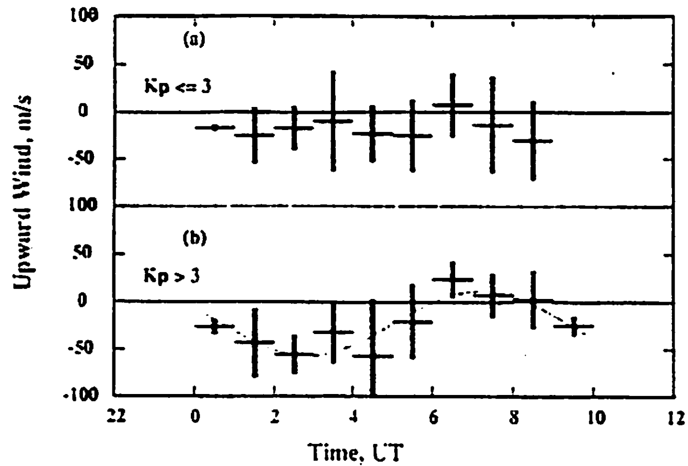

Fig. 5. Vertical wind averages for 1-h bins containing all the bistatic measurements from geomagnetically quiet nights (a) and disturbed nights (b). The vertical bars show the uncertainty in the average, most of which is due to the night-to-night variability.

the data are negative (corresponding to a downward wind). The points for each night were averaged as if there were no diurnal variation using the variance of the individual points for weighting to determine a mean night-time vertical wind: the result is shown by the heavy error bar near the ordinate.

Figure 4b displays an example of data obtained on a geomagnetically disturbed night, 23 August, when K_p values ranged between 7 and 8 during the observing period. The 630 nm intensity remained elevated above normal quiet-night values throughout the period. The vertical winds are stronger and average more strongly negative than on the quiet nights.

The set of data for quiet nights was binned in 1 hour intervals and averaged in order to look for diurnal variations. The resulting data are shown in Fig. 5a. Here the horizontal bar of the symbol represents the mean wind derived from an average of the measure-

Biondi & Sipler
1985

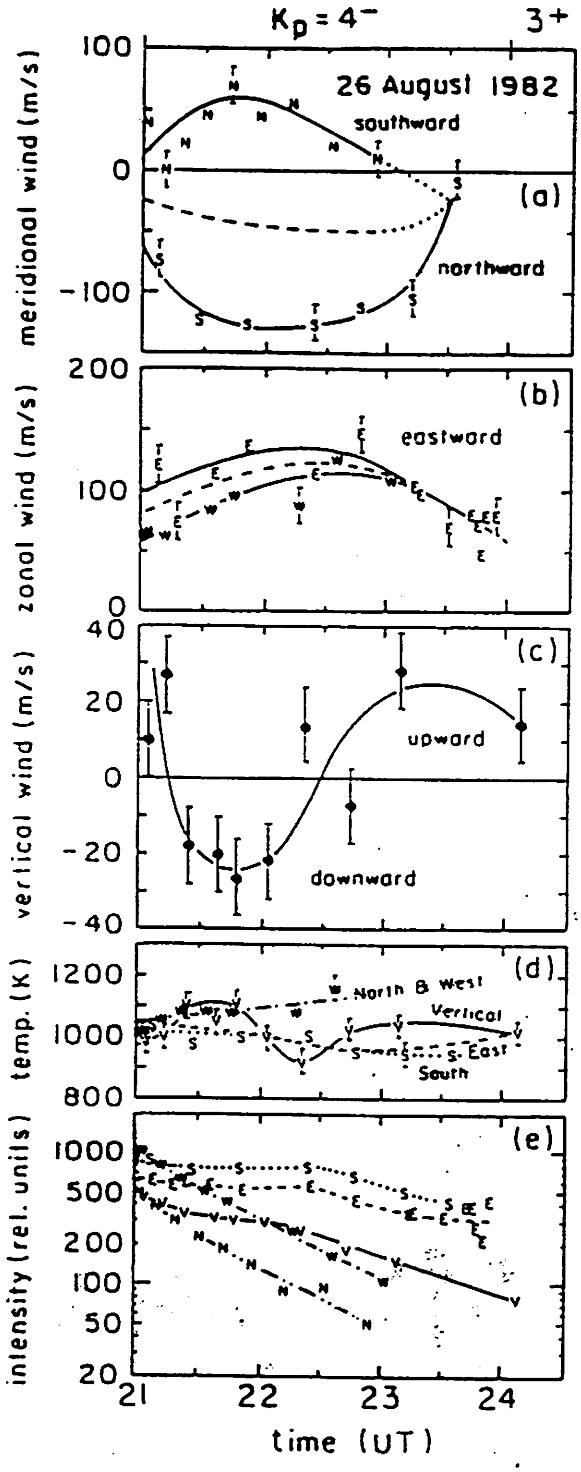

FIG. 2. MEASURED MERIDIONAL, ZONAL AND VERTICAL WINDS, NEUTRAL TEMPERATURES AND 630.0 nm INTENSITIES AS FUNCTIONS OF TIME ON 26 AUGUST 1982, WHEN $\Sigma K_p = 27$.
The 3-h K_p indices are indicated at the top of the figure. The symbols N, S, E, W and V indicate the observation directions: the North and East data points have been omitted from the temperature scale for clarity. Typical error bars are shown on some of the data points.

Biondi + Sipler, 1984

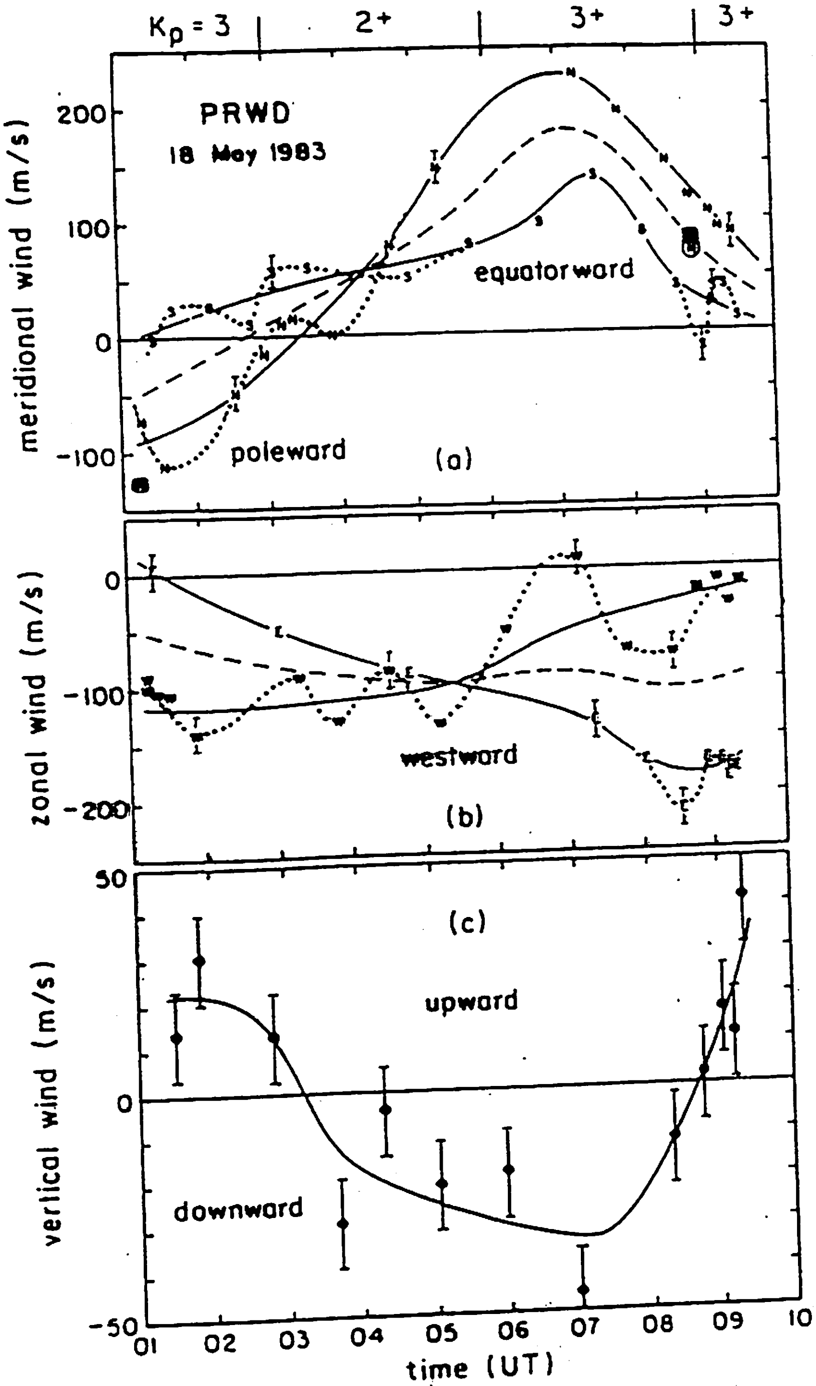

Fig. 1 Measured wind components on 18 May 1983. The letters refer to the observing azimuth at 20° elevation (except: boxed letters, 30° elevation and circled letter, 45° elevation). Typical error bars are shown on some data points.

Herrero and Meriwether, 1995

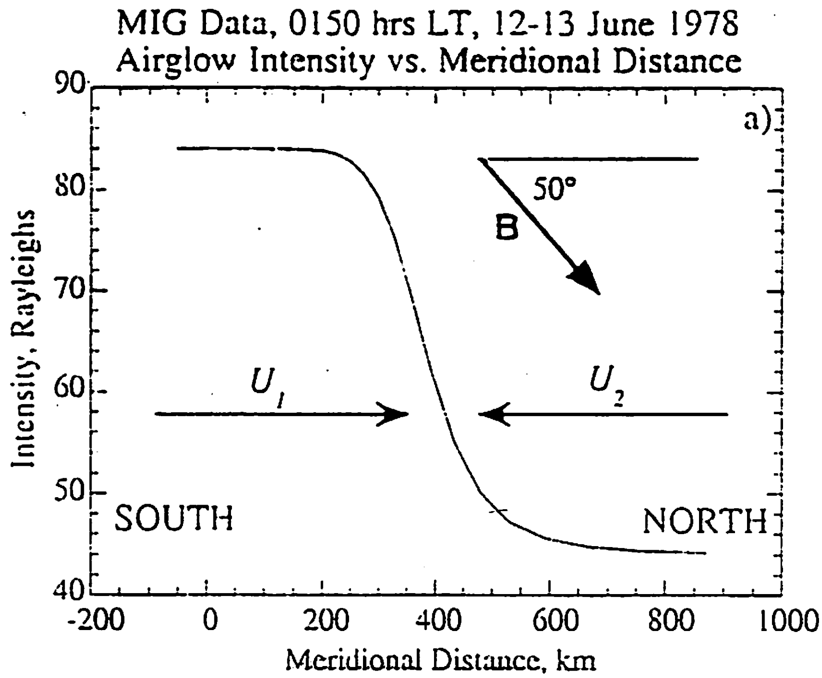

Fig. 2 a) Meridional intensity distribution along y at the emission layer height, taken from Figure 1. An average emission layer altitude of 250 km was assumed, ignoring the variation with height of the layer that occurs due to the wind gradient.

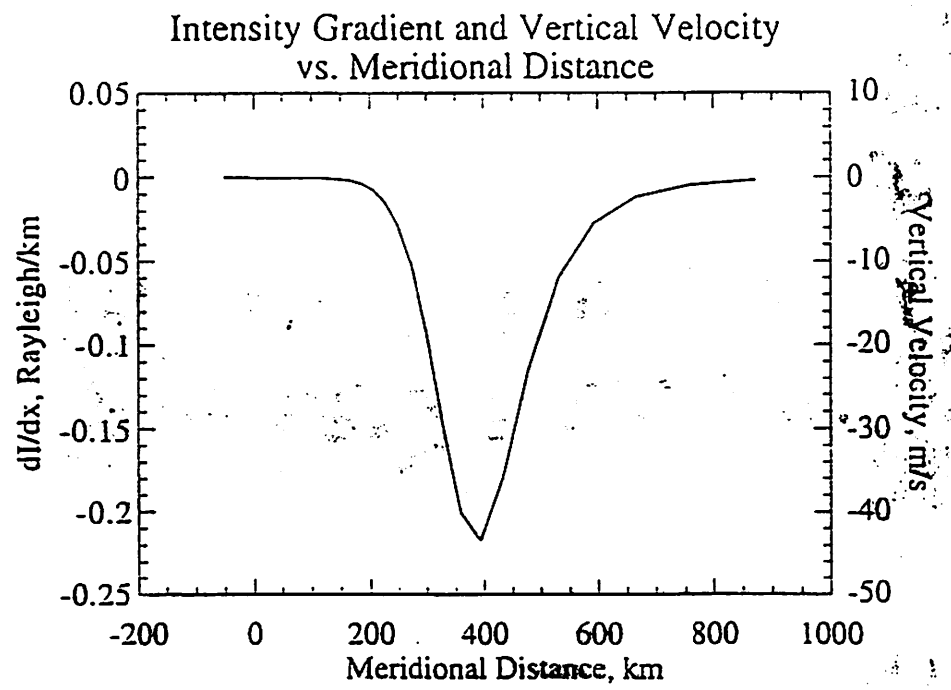

Fig. 2 b) Airglow intensity gradient obtained from a) with scale on the left hand ordinate; scale on right hand indicates estimated vertical wind as described in the text.

Burnside et al., 1981

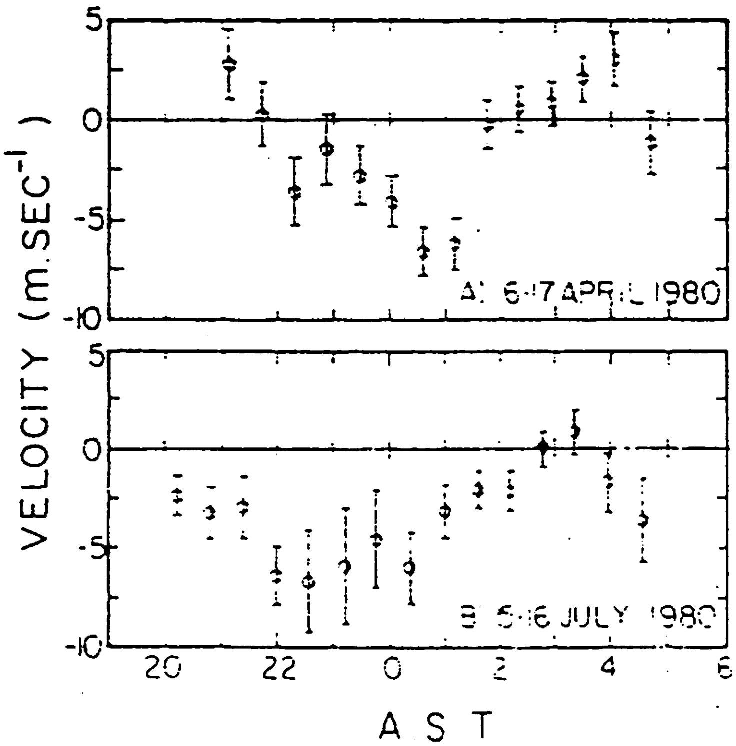

d
nd
n-
d-

Fig. 8. The inferred vertical wind velocity for the same two nights as shown in Figure 6. A scale height of 50 km was assumed in obtaining these results. Negative values correspond to downward flow.

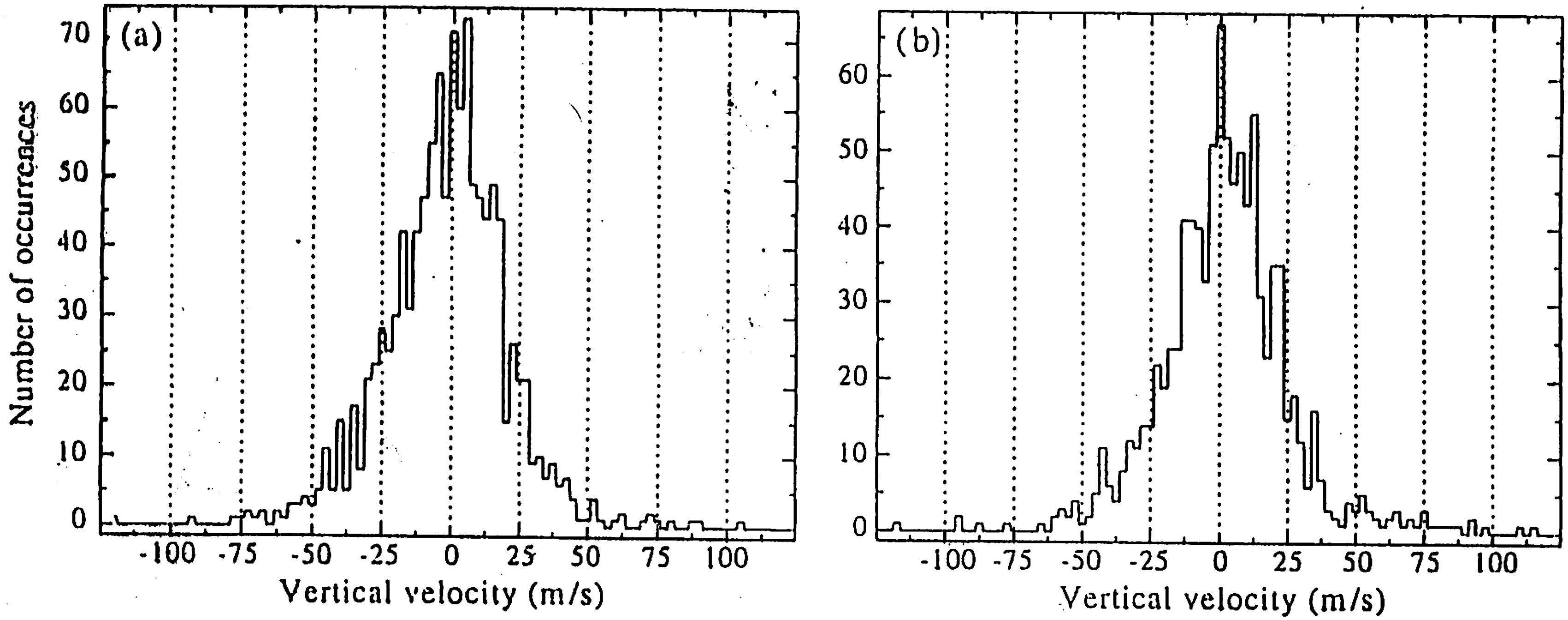

Fig. 2. (a) Distribution of occurrences of vertical wind speeds calculated from all zenith spectra whose central time of aquisition occurred when the local three-hourly magnetic K-index was 3 or less. Each speed "bin" is 2.5 m s^{-1} wide. The distribution represents a total of 1137 individual measurements. (b) As for (a), but calculated from zenith spectra gathered during times when the local three-hourly magnetic K-index was greater than 3. In this case, 959 measurements were used.

Conde & Dyson, 1995

Condor Dyson, 1995

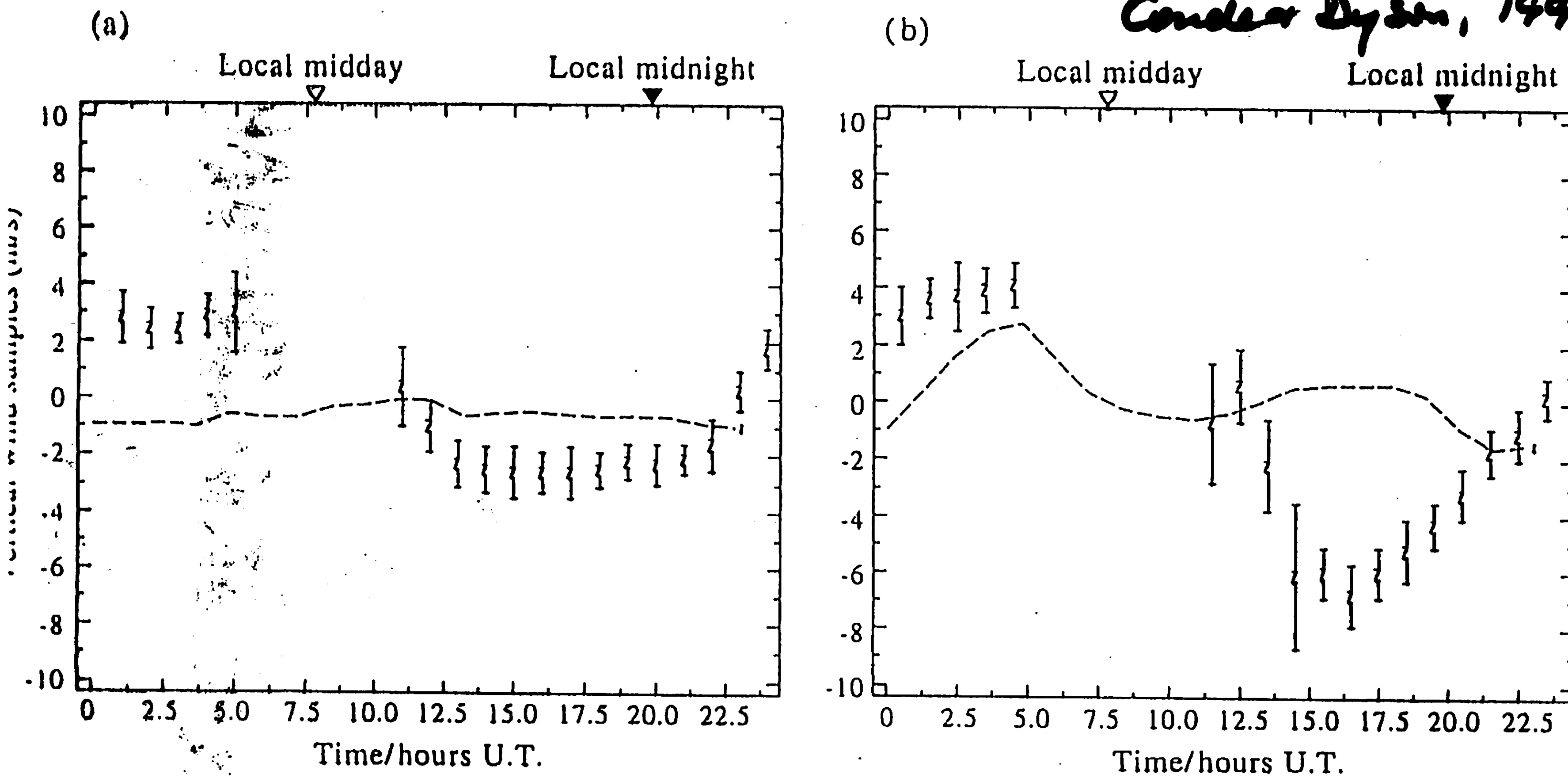

Fig. 1. (a) Averaged vertical wind values as a function of Universal Time calculated from all zenith spectra whose central time of aquisition occurred when the local three-hourly magnetic *K*-index was 3 or less. Error bars indicate the one-sigma uncertainty in estimating each averaged value. The dashed curve indicates the vertical wind predicted by a run of the University College London thermospheric general circulation model. Model runs are identified by a three-character code; in this case, output is from runcode A84, which represents quiet magnetic conditions around 21 June with a 10.7 cm solar radio flux index of 185. (b) As for (a), but calculated from zenith spectra gathered during times when the local three-hourly magnetic *K*-index was greater than 3. In this case, the model output is from run code GB2, which is similar to A84 but for disturbed magnetic conditions.

(a)

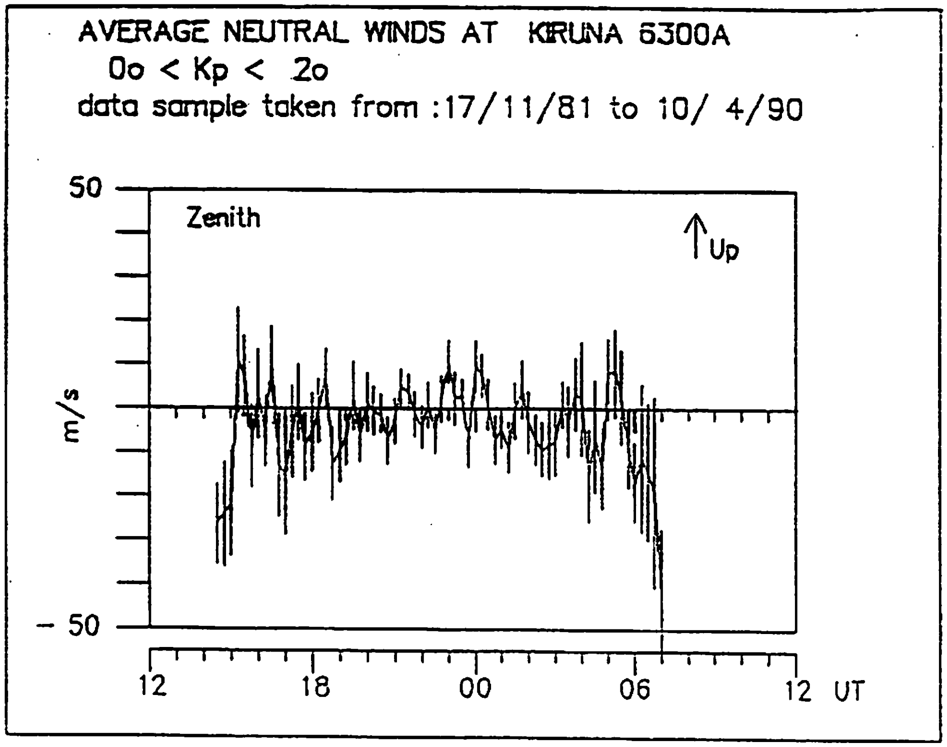

(b)

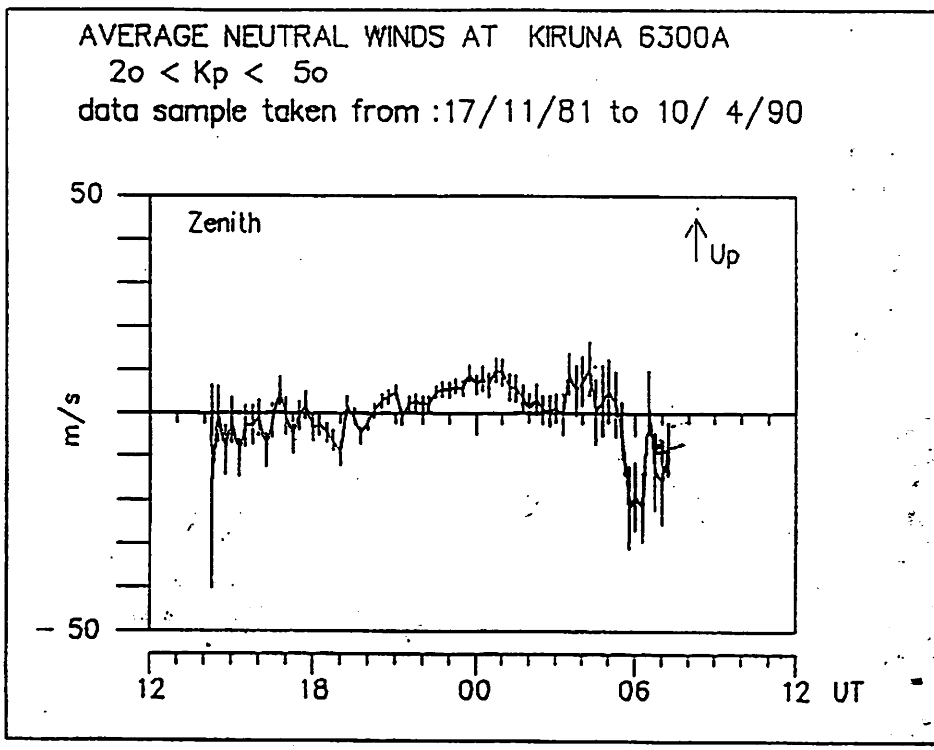

Fig. 4. The mean vertical wind in the thermosphere above Kiruna as a function of geomagnetic activity and Universal Time during the period November 1981 until April 1990. Fig. 4(a) is for $0^{\circ} < K_p < 2^{+}$, while Fig. 4(b) is for $2^{+} < K_p < 5^{\circ}$.

Aruliah & Rees, 1995

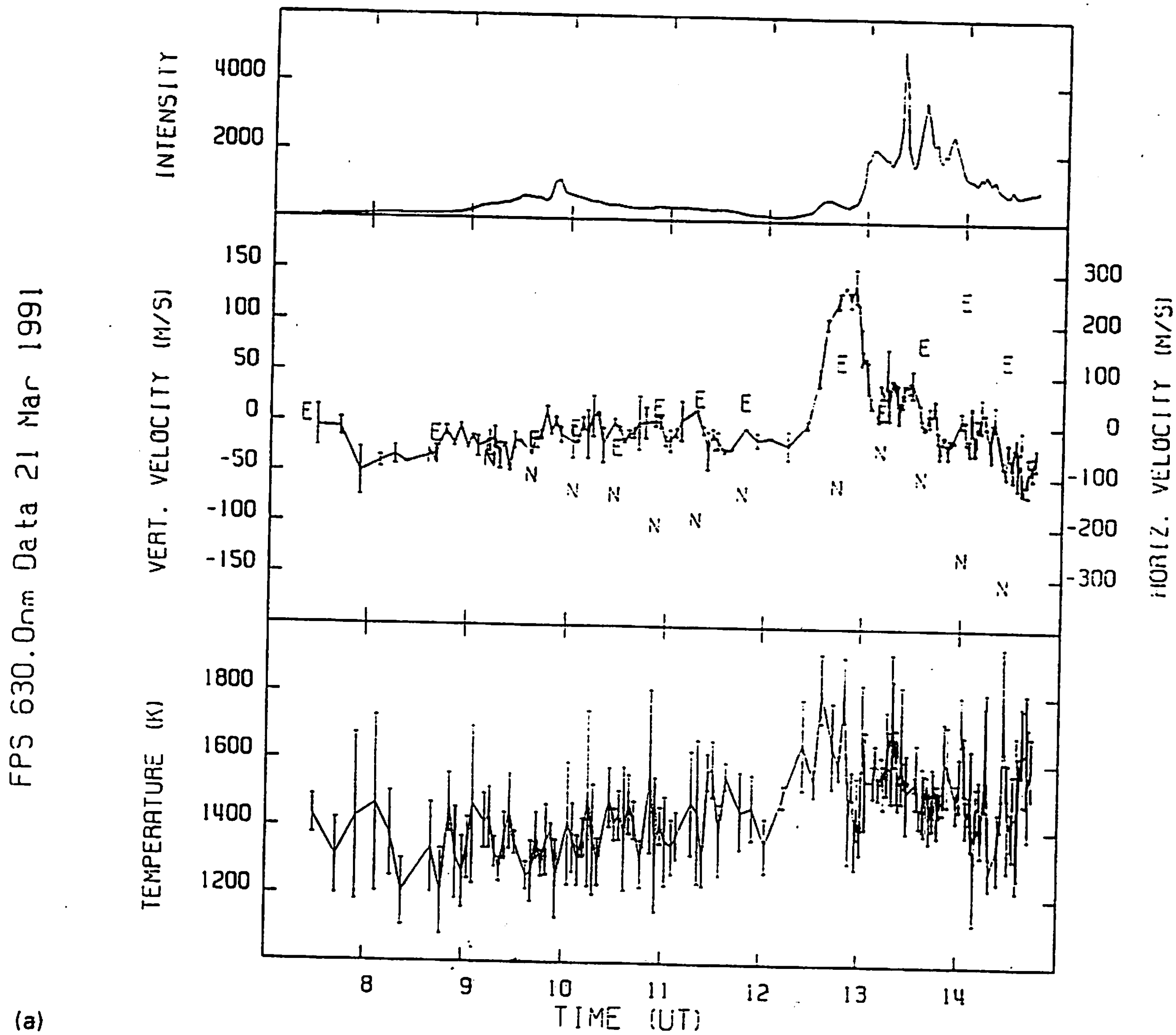

Fig. 2(a).

Price et al., 1995

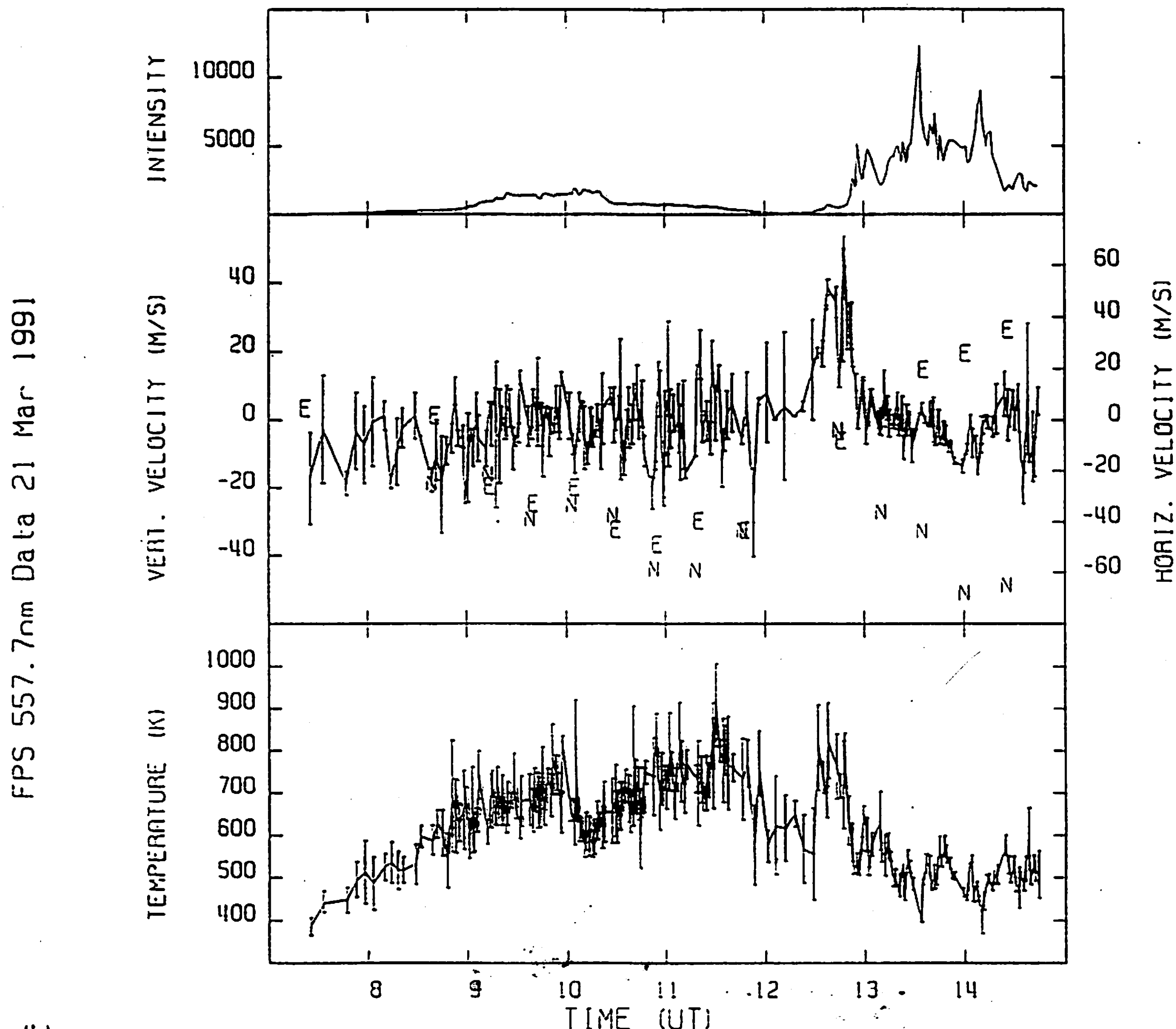

(b)

Fig. 2. 21 March 1991: FPS measurements of (a) the λ630 nm emission and (b) the λ558 nm emission showing an upwelling at around 12.30 UT. The horizontal time axis is common to all three panels, and the

Price et al., 1995

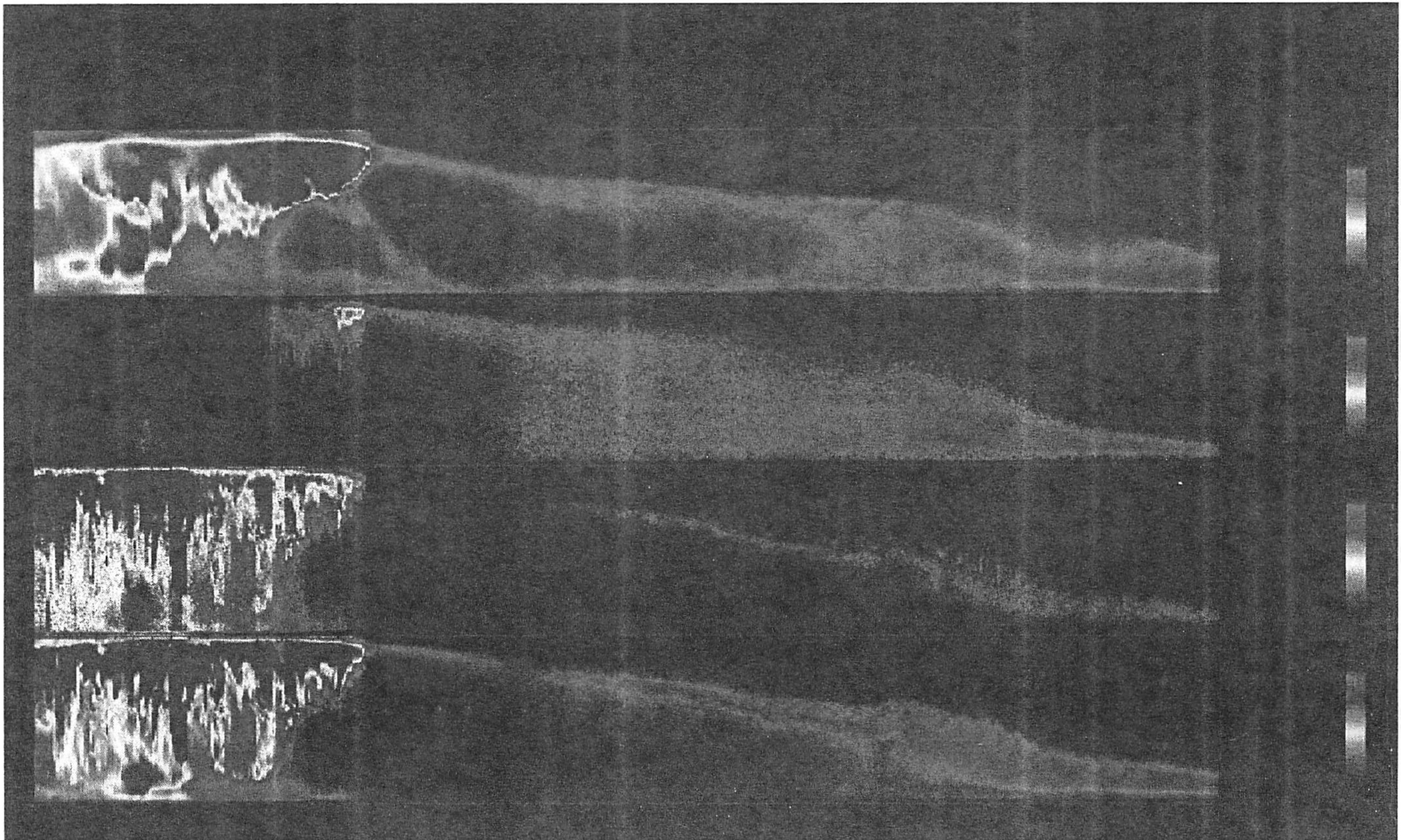

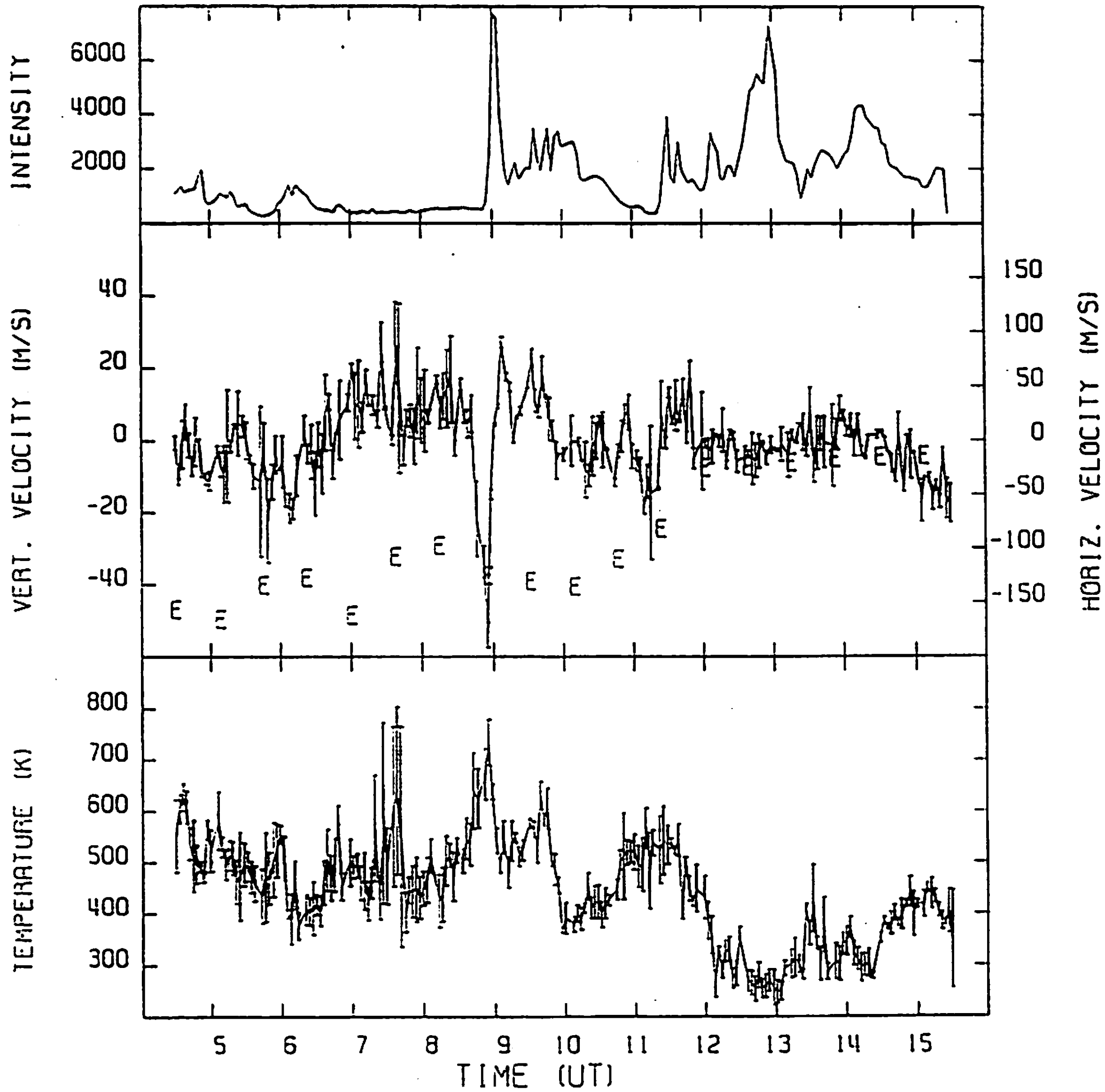

b)

Fig. 4. 10 March 1991. FPS

Price et al., 1995

Fabry–Perot spectrometer observations

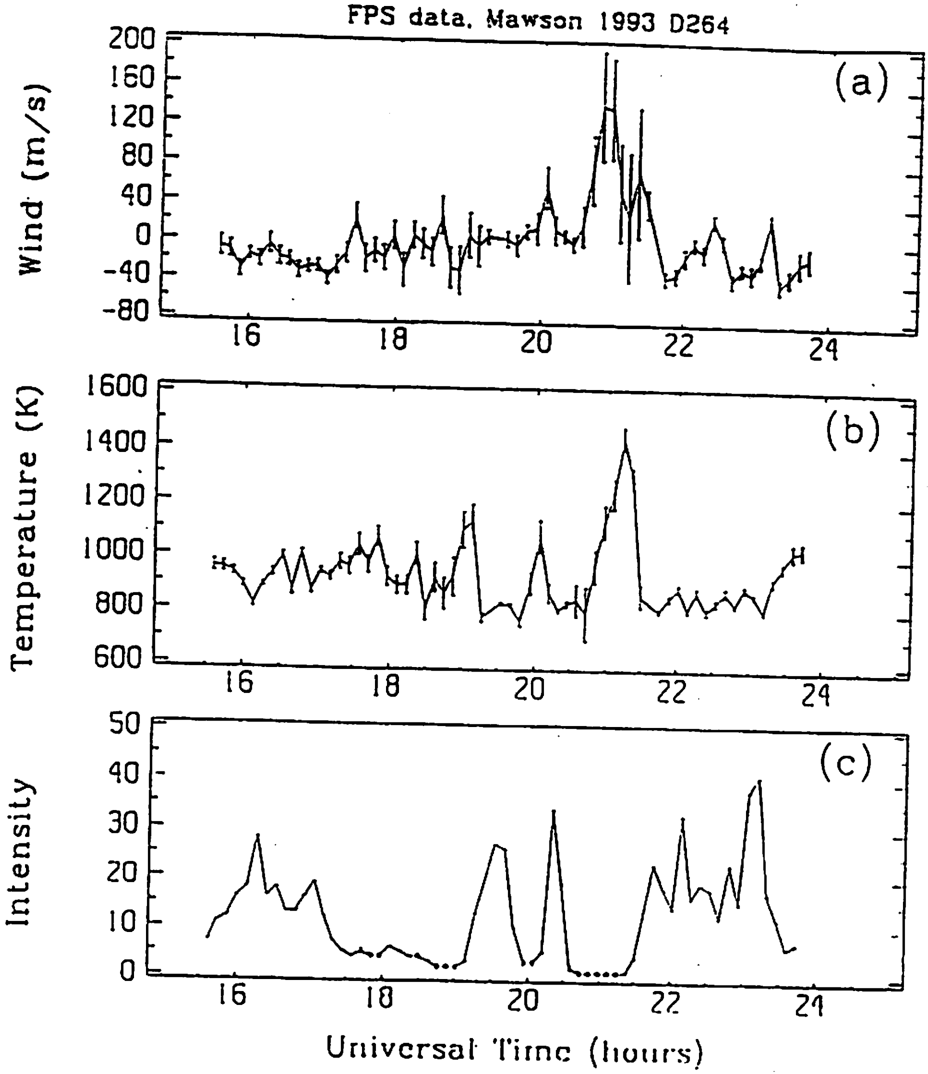

Fig. 2. As for Fig. 1, but for DOY 264.

Innis et al., 1996

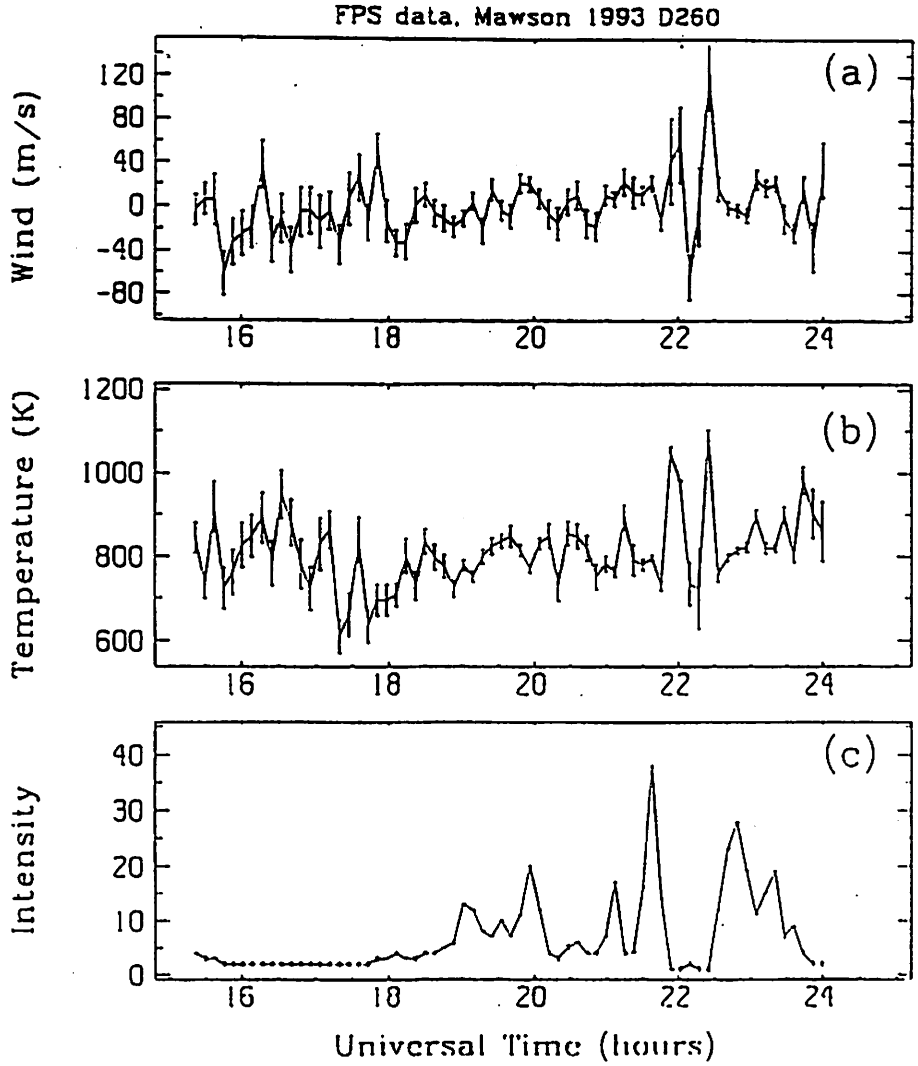

Fig. 1. Time series of wind (a), temperature (b), and relative intensity (c), from Mawson FPS zenith data for DOY 260 from the oxygen λ630 nm emission.

Innis et al., 1996

Rees et al., 1984

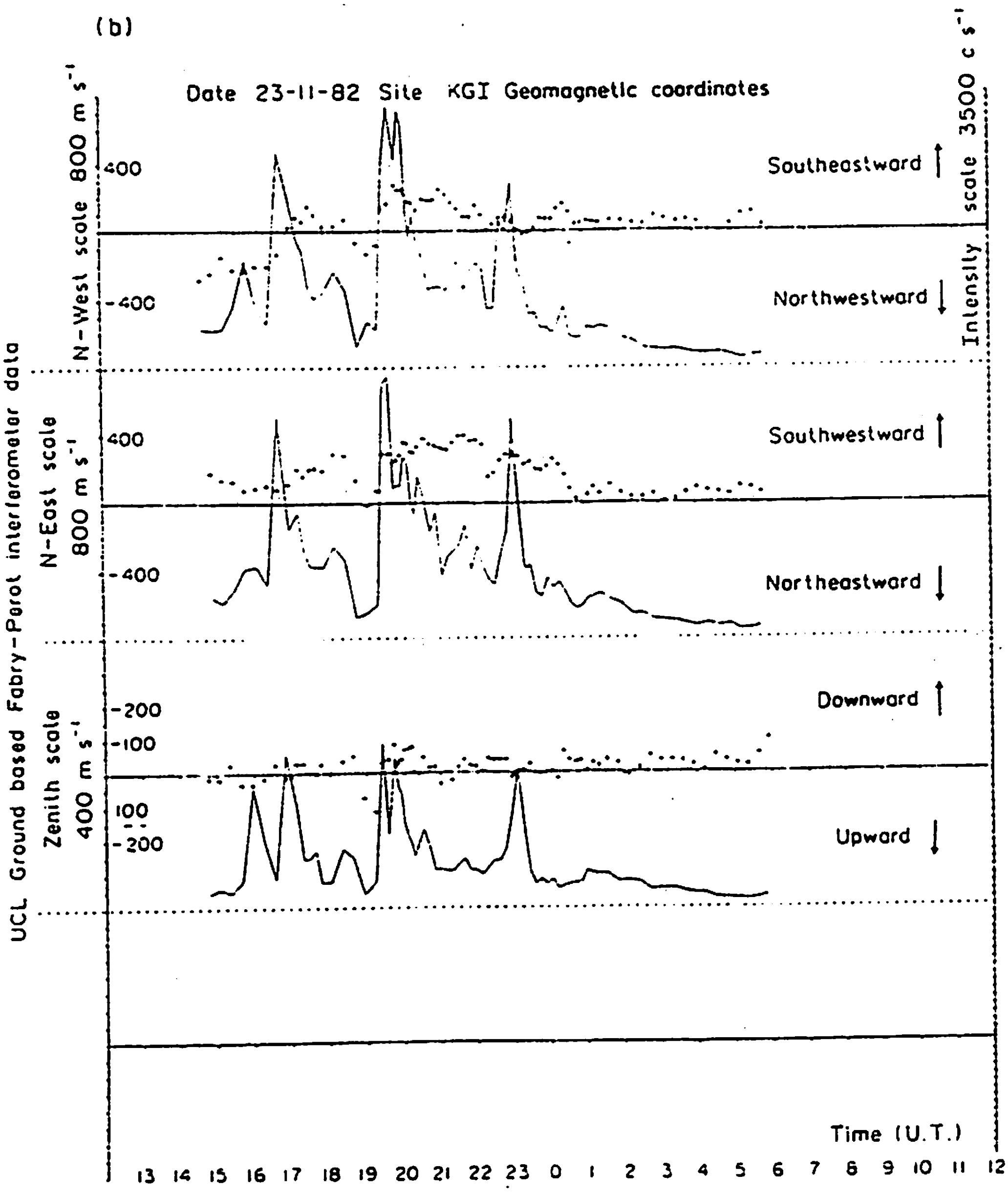

FIG. 4. THERMOSPHERIC WINDS OBSERVED IN THE N, NE, E, S, W, NW AND VERTICAL DIRECTION FROM KIRUNA GEOPHYSICAL INSTITUTE ON THE NIGHT OF 23/24 NOVEMBER 1982.

The major focus of interest is the correspondence between changes observed in each of the viewing directions in the period 18.00–20.00 U.T. before, during and after the strong disturbance near 19.00 U.T. Observed winds are indicated by the crosses (+), and the OI 630 nm intensity by the continuous line.

Wardill + Jacka, 1986

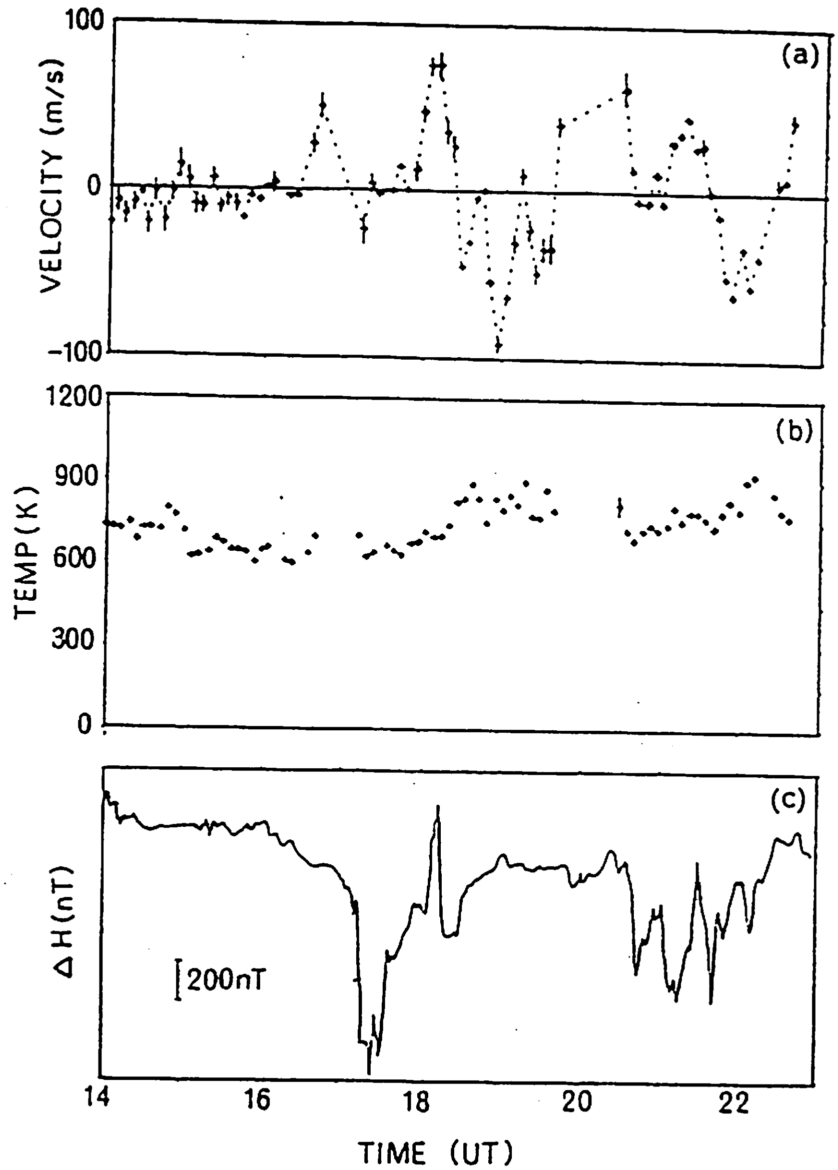

Fig. 1. Thermospheric vertical velocity (a), temperature (b) and H component of the local magnetogram (c) for 24 May 1983.

Crickmore, 1993

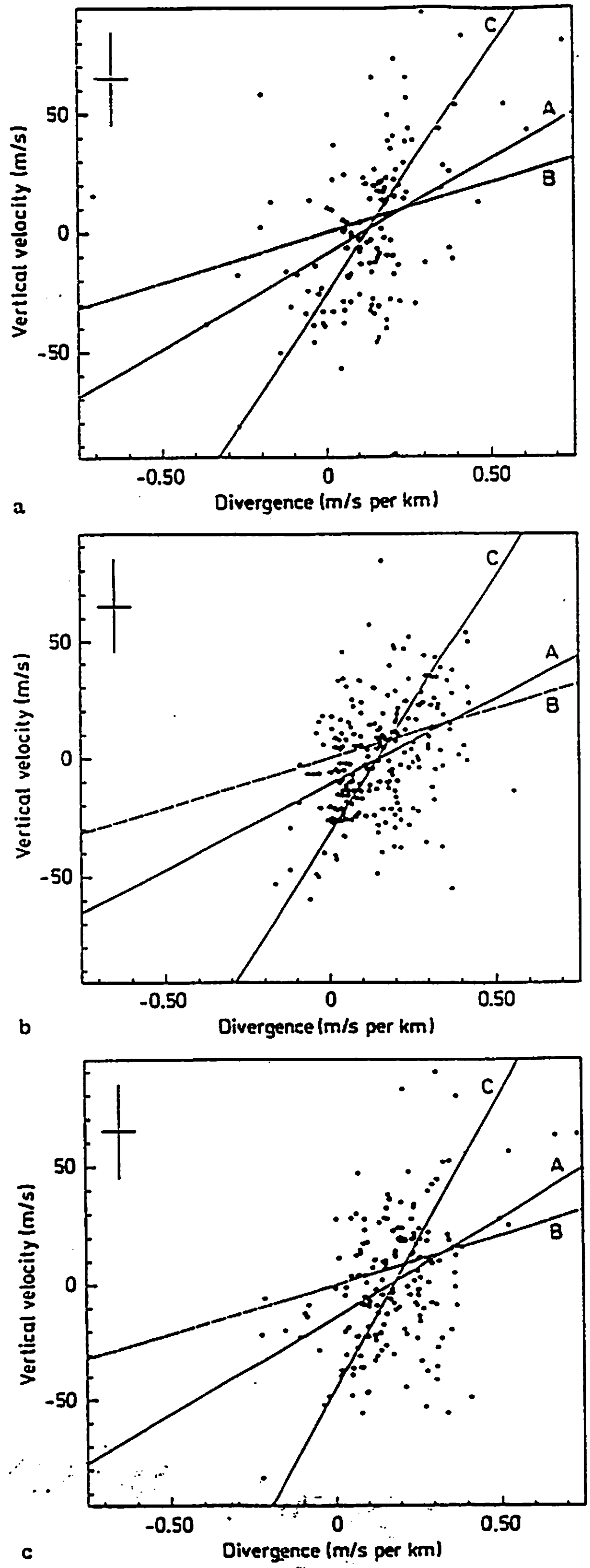

Fig. 2. a Vertical wind velocity versus horizontal divergence measured at Halley during 1988. The positive Y-axis is the upward wind. *Line A* is the linear regression line using the divergence as the independent variable. *Line B* is that predicted theoretically by the method of Burnside *et al.* *Line C* is the best fit obtained by minimizing the sum of the squares of the perpendicular distance between the line and the points. Typical *error bars* are shown in the top left of the figure. b and c as for a but with data for 1989 and 1990 respectively


09 UT on November 17, 1996

Hernandez + Roble, 1978

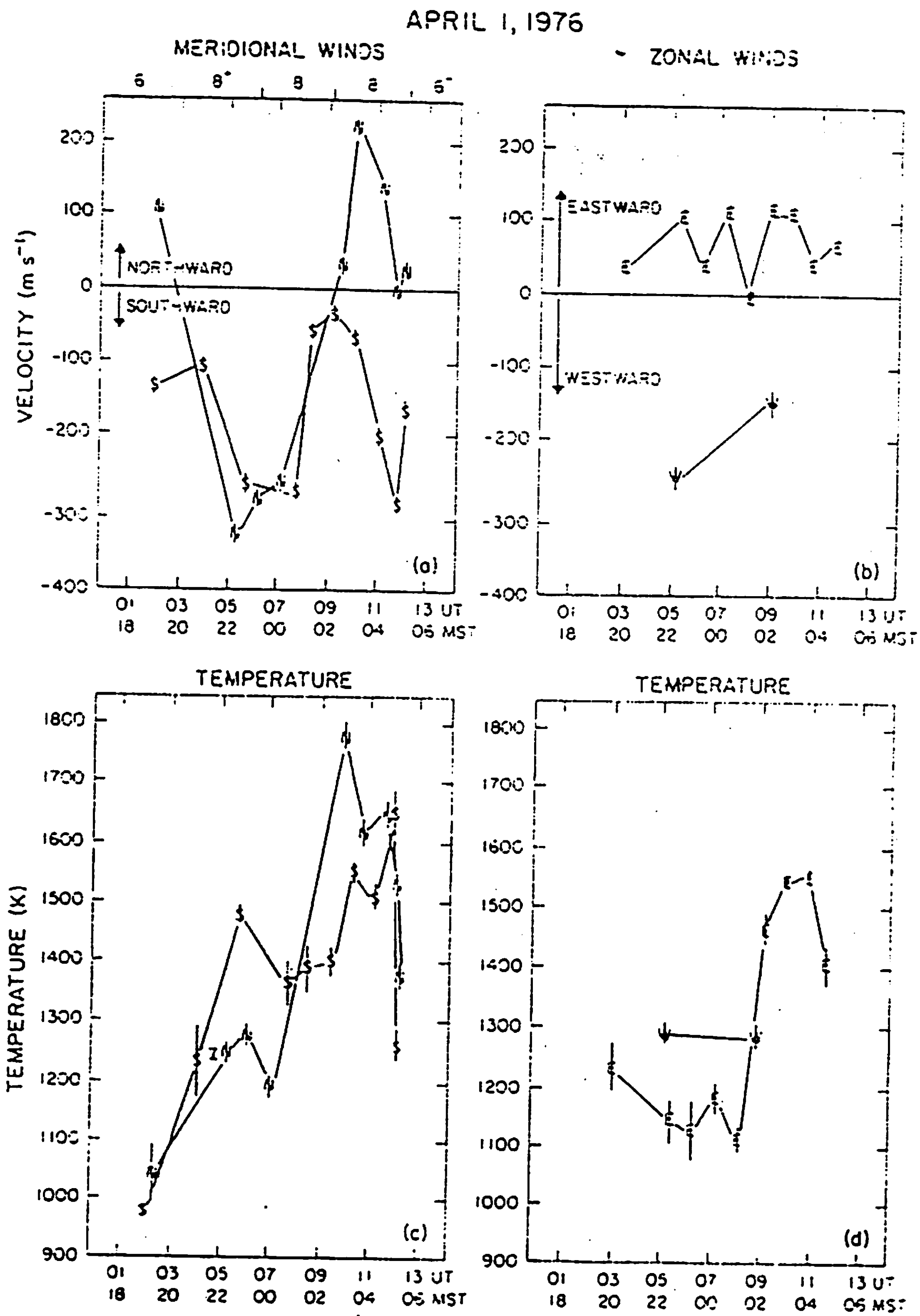

Fig. 1. Nighttime measurements of (*a*) meridional winds (m s^{-1}), (*b*) zonal winds (m s^{-1}), (*c*) neutral gas temperatures in the north-south direction, and (*d*) neutral gas temperatures in the east-west direction over Fritz Peak Observatory during the geomagnetic storm on April 1, 1976. The time is given in universal time (UT) and mountain standard time (MST). The letters for each data point indicate the direction from Fritz Peak Observatory where the measurement was made: N (north), S (south), E (east), W (west), and Z (zenith). The bars through the letters give the standard deviation of the measurements. The data points in each direction are connected by a solid line.

Smith & Hernandez, 1995

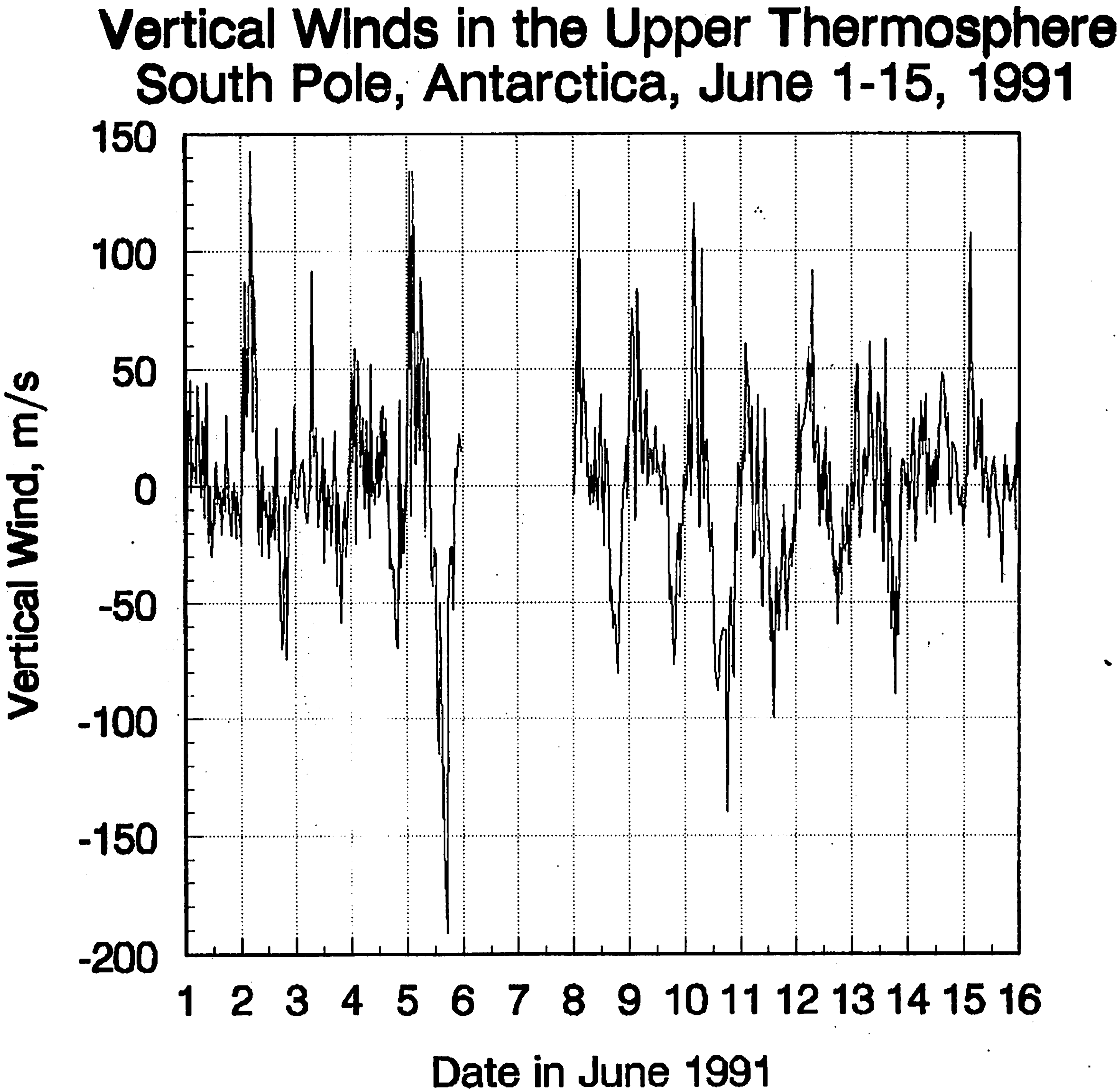

Smith & Hernandez, 1995

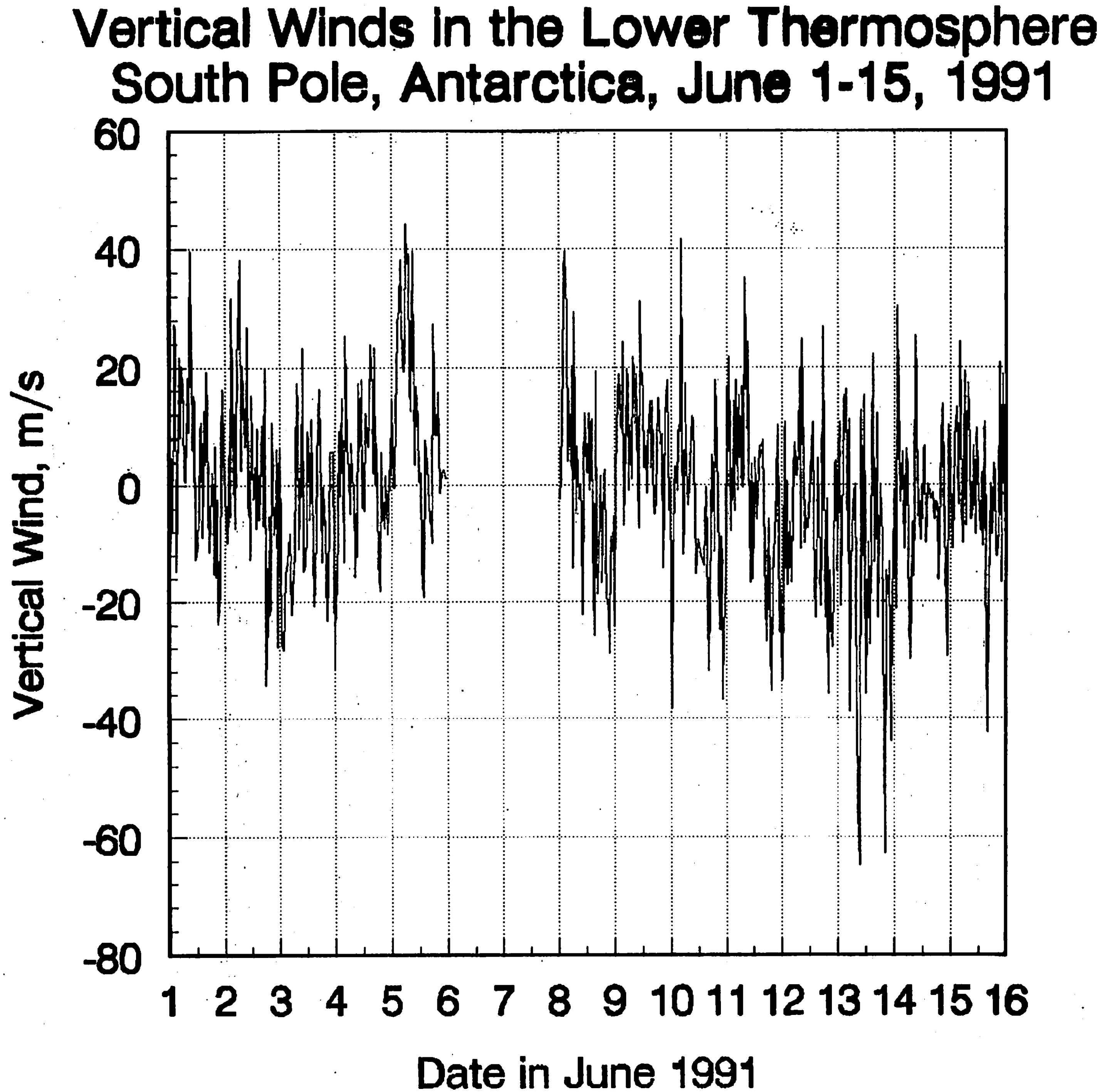

Smith + Hernandez, 1995

South Pole Vertical Velocities
June 5 1991

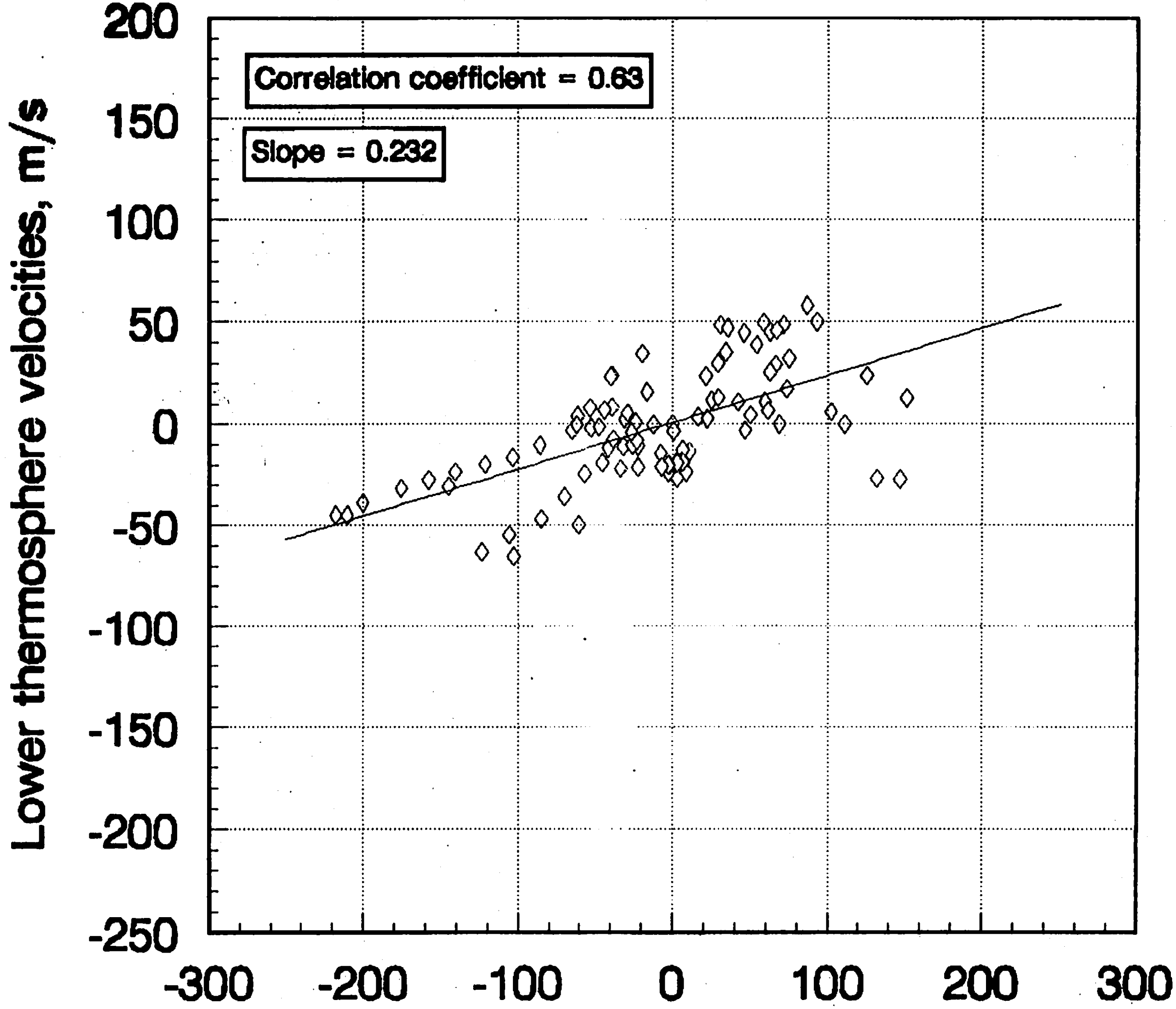

Upper Thermospheric Velocities, m/s

Smith & Hernandez, 1995

Vertical Wind Extremes om the Upper Thermosphere Variation with KpSum

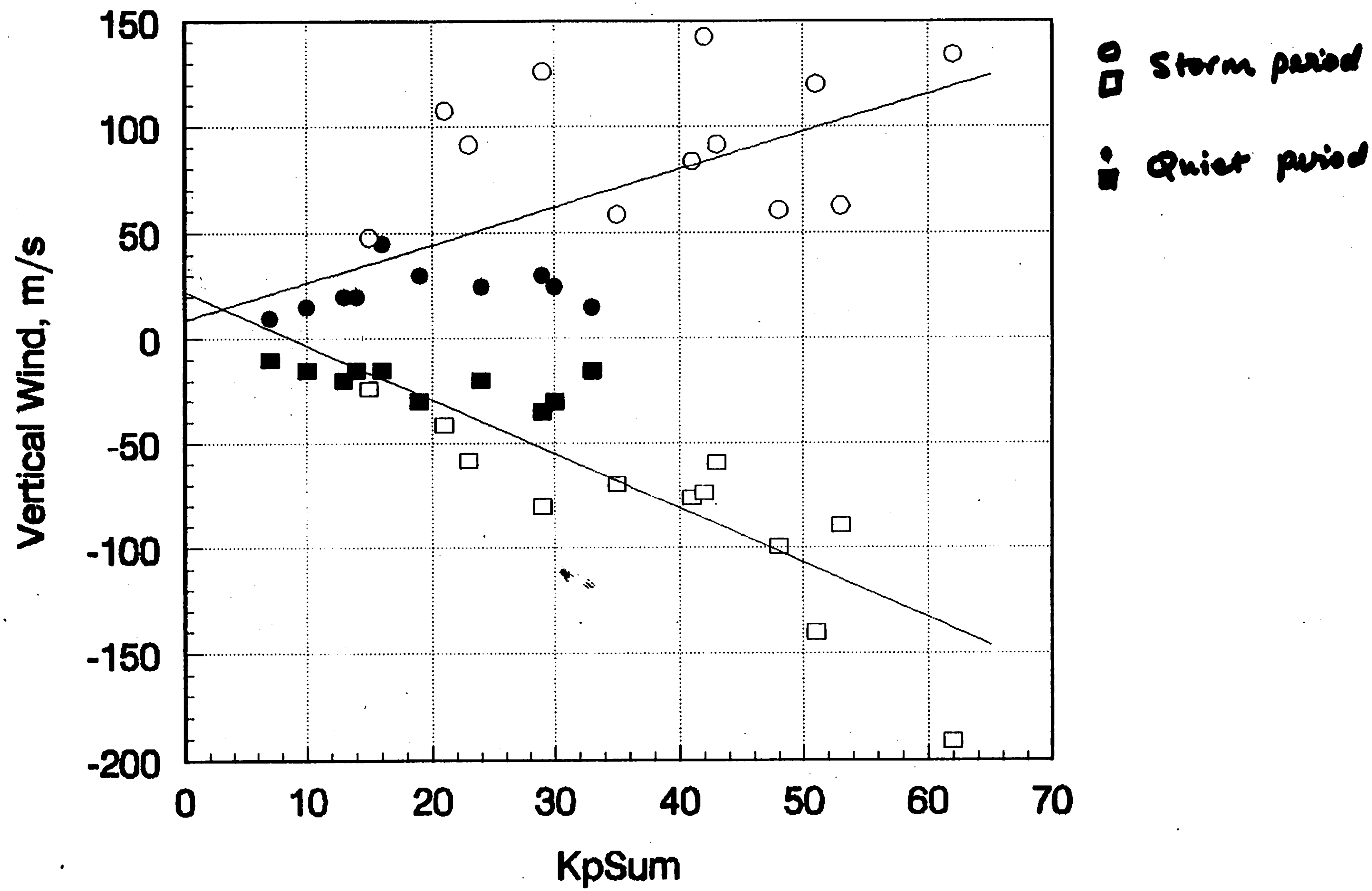

Rees et al., 1984

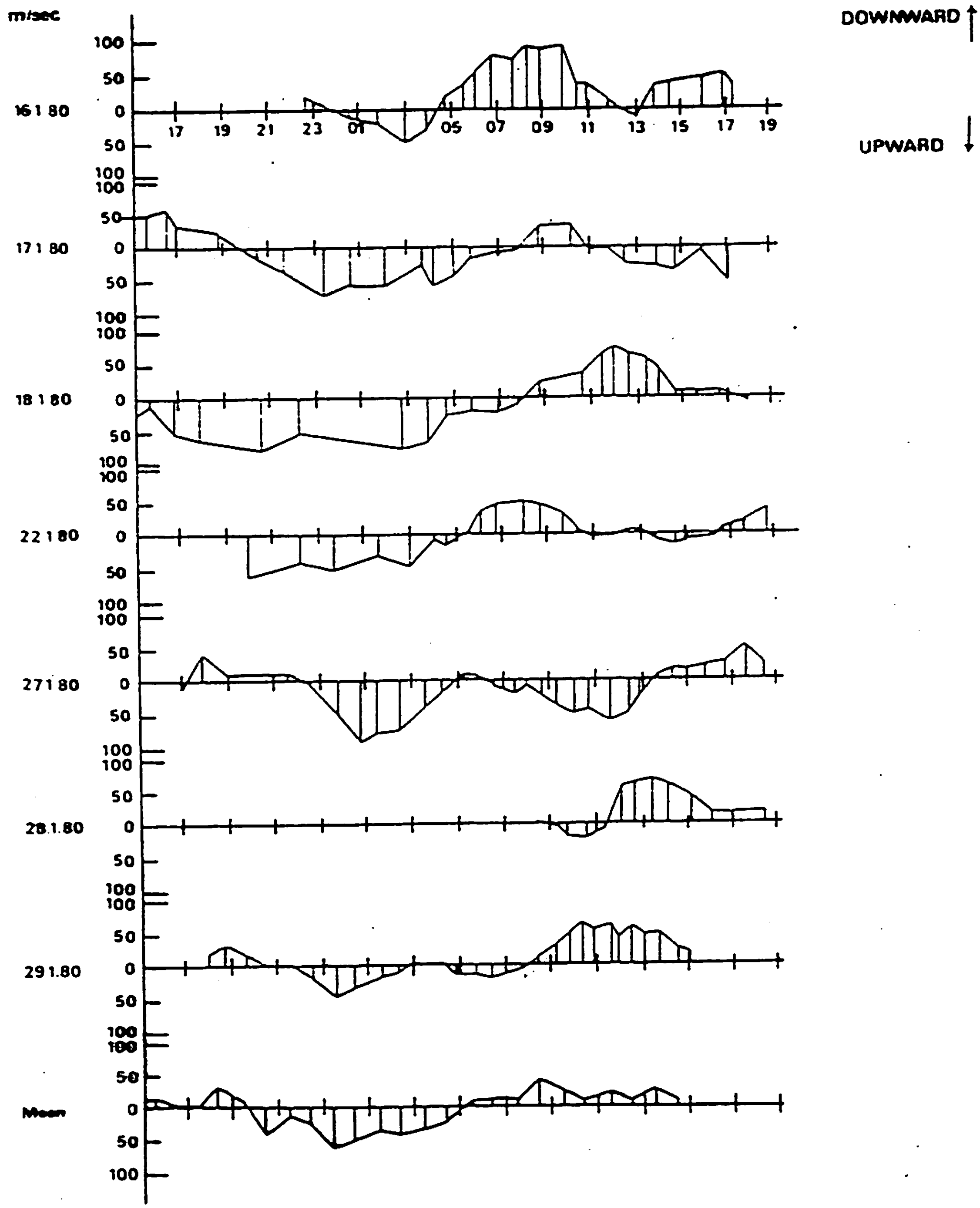

FIG. 2. DATA FROM LONGYEARBYEN, SPITZBERGEN, IN JANUARY 1981 SHOWING THE VERTICAL COMPONENT OF THE THERMOSPHERIC WIND AS A FUNCTION OF U.T. PLOTTED ON A COMMON TIME AXIS.
The seven upper plots cover individual days and the lowest plot shows the mean vertical wind for these days.

SUMMARY OF OBSERVATIONS

0. VERTICAL WINDS FOUND EVERYWHERE > few m/s

1. LARGE (< 150 m/s), SHORTLIVED (30-60 MINS) <u>UPWARD</u> WINDS OBSERVED AT HIGH LATITUDES

2. LARGE (< 150 m/s), SHORTLIVED (30-60 MINS) <u>DOWNWARD</u> WINDS OBSERVED AT HIGH LATITUDES

   — but longer-lived at South Pole

3. WAVES ± 40 m/s SEEN GLOBALLY

4. HORIZONTAL EXTENT OF LARGE EVENTS ~ 400 km IN MERIDIAN.

5. SOME EVIDENCE THAT $W = (\text{const})\, \nabla_H \cdot \vec{U}$

   but const $\neq H$ at HALLEY

DATA SHEET

120km $T = 400K$ $n = 10^{17} m^{-3}$ $H = 10km$

250km $T = 1200K$ $n = 10^{15} m^{-3}$ $H = 60km$

ESTIMATORS

- Number of particles in column of unit area $N = \int n_0 e^{-h/H} dh = n_0 H$

  $H = kT/mg$

- Time for gravity wave to travel vertically 120–250km

  – assume speed 100m/s, $\tau = \frac{130 \times 10^3}{100} \simeq 1300s$

- Time for acoustic wave to travel vertically 120–250 km

  – assume speed 1km/s, $\tau = \frac{130 \times 10^3}{1000} \simeq 130s$

- Time for change due to steady vertical flow in vertical column:

$$\frac{1}{\tau} = \frac{1}{p}\frac{dp}{dt} = \frac{1}{p}\cdot\frac{dp}{dh}\cdot\frac{dh}{dt}$$

$$= \frac{1}{p}\cdot\frac{-p}{H}\cdot w$$

$$\therefore \quad \tau = H/w$$

- Thermal energy present in unit column of thermosphere above 120km:

$$\Phi = nH.\frac{3}{2}kT = 10^{17} \times 10^{4} \times 1.5 \times 1.4 \times 10^{-23} \times 400$$

$$\doteq 10J$$

for substantial change, another 10J required (eg 50mW m^{-2} for 200s)

SOURCES OF VERTICAL WIND

1. ESCAPE OF LIGHT GASES H + He
2. DIFFUSIVE ADJUSTMENT TO 'IN SITU' CHEMICAL CHANGE
3. HEATING (COOLING) — w_B
4. DIVERGENCE IN HORIZONTAL FLOW — w_D

$$(w = H \nabla_h . \vec{U})$$

This tutorial will not consider 1 or 2.

Total vertical wind $W = W_B + W_D$

or $$= \left(\frac{\partial h}{\partial t}\right)_p + \left(\frac{1}{\rho g}\right)\frac{\partial p}{\partial t}$$

rate of rise of constant pressure surface

pressure changes due to divergent horizontal flow.

ESTIMATORS CONT'D

CONNECTION BETWEEN VERTICAL WIND & HORIZONTAL DIVERGENCE

— through continuity equation.

(Burnside et al., 1981)

Integrate continuity equation & use barometric equation:

$$\frac{\partial p}{\partial t} = -g \int_h^\infty \left[\frac{\partial}{\partial x}(\rho u) + \frac{\partial}{\partial y}(\rho v) \right] dz + g(\rho w)_h$$

— evaluate by assuming: isothermal atmosphere above airglow

horizontal wind independent of height.

$$\frac{\partial p}{\partial t} = -p \left[\frac{\partial u}{\partial x} + \frac{\partial v}{\partial y} \right] + g(\rho w)_h$$

Further assume rate of change of pressure at level of airglow is negligible.

$$\therefore \quad w = H \left[\frac{\partial u}{\partial x} + \frac{\partial v}{\partial y} \right]$$

SLOW VERTICAL MOVEMENT

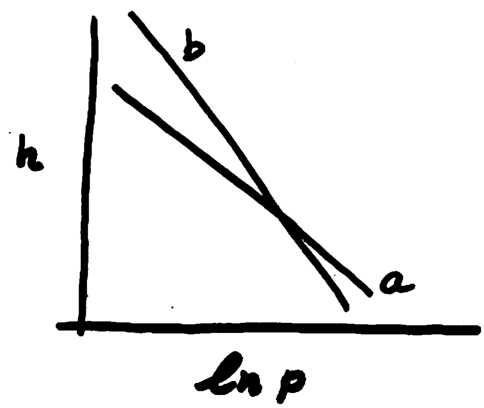

Go from a to b by a quasi-static process.

Diurnal temperature variation in F-region: amplitude 300K

mean rate of rise: $\frac{300}{12\times 60\times 60} = \frac{1}{144}\ \mathrm{K\,s^{-1}}$

heating rate/particle $= \frac{3}{2}k \cdot \frac{1}{144} \simeq \frac{k}{100}\ \mathrm{J\,s^{-1}}$

heating rate/unit column $= nH.\frac{k}{100} = 10^{15}\times 4\times 10^{4}\times 1.4\times 10^{-23}\times 10^{-2}$

$\simeq 6\ \mu\mathrm{W\,m^{-2}}$

Convert $6\ \mu\mathrm{W\,m^{-2}}$ to potential energy — how fast will column rise?

$\rho g H.h = 6\mu J$ $\quad$ h = vertical displacement in 1 sec

$\rho = 10^{15}\times 16\times 1.7\times 10^{-27} = 2.5\times 10^{-11}\ \mathrm{kg\,m^{-3}}$

$$\underline{h} = \frac{6\times 10^{-6}}{2.5\times 10^{-11}\times 10\times 6\times 10^{4}} \doteq \underline{0.5\ \mathrm{m}}$$

Hence estimate of vertical velocity $\underline{\underline{0.5\ \mathrm{m/s}}}$

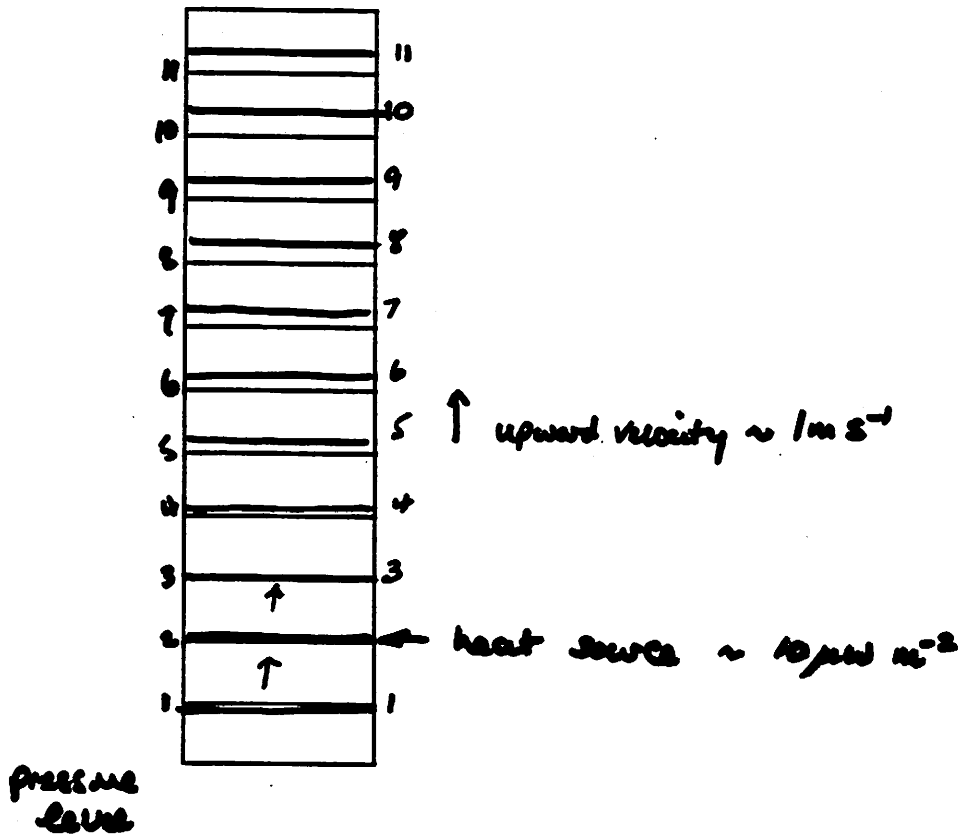

SINGLE ATMOSPHERIC COLUMN.

SLOW EXPANSION

DEPARTURE FROM HYDROSTATIC EQUILIBRIUM (1)

$p - dp$

Δh

p

$dp = \rho g \Delta h$ at exact equilibrium

if $dp \neq \rho g \Delta h$ then there is vertical acceleration.

Navier Stokes: $\frac{D\vec{U}}{Dt} + 2\vec{\Omega}\times\vec{U} = -\frac{1}{\rho}\nabla p + \nu(\vec{V}-\vec{U}) + \frac{\mu}{\rho}\nabla^2\vec{U} + \vec{g}$

taking selected terms in vertical. $\underline{\frac{\partial w}{\partial t} = -\frac{1}{\rho}\frac{\partial p}{\partial z} + g}$

→ SLOW vertical movement — mean vertical speed few m/s

— $\frac{\partial w}{\partial t}$ needs to be about $g/10^4$

(quasistatic case)

→ FAST vertical movement — mean vertical speed 100 m/s

— $\frac{\partial w}{\partial t}$ needs to be about $g/10^2$

eg. if uniform acceleration occurred from 120 km → 250 km resulting in 100 m/s after starting from rest then ($v^2 = 2fs$)

$$\frac{\partial w}{\partial t} = \frac{10^4}{260\times 10^3} \simeq \frac{1}{26}\ m\,s^{-2} \sim g/200$$

Hence unbalancing the hydrostatic equation by 1% is sufficient to generate observed winds in this simple approximation.

DEPARTURE FROM HYDROSTATIC EQUILIBRIUM (2)

Add in dynamic pressure (ρw^2) — needs to be a dynamic pressure gradient to be effective

$$\frac{\partial w}{\partial t} = -\frac{1}{\rho}\frac{\partial p}{\partial z}\bigg|_b - \frac{1}{\rho}\frac{\partial p}{\partial z}\bigg|_d + g$$

this term caused by vertical flow impressed by divergence of horizontal flow.

if $w = 100\,\mathrm{ms^{-1}}$ at 250km then time to stabilize $= \frac{60 \times 10^4}{100}$

$= \underline{6000\,s}$

Hence for most cases stabilization never occurs

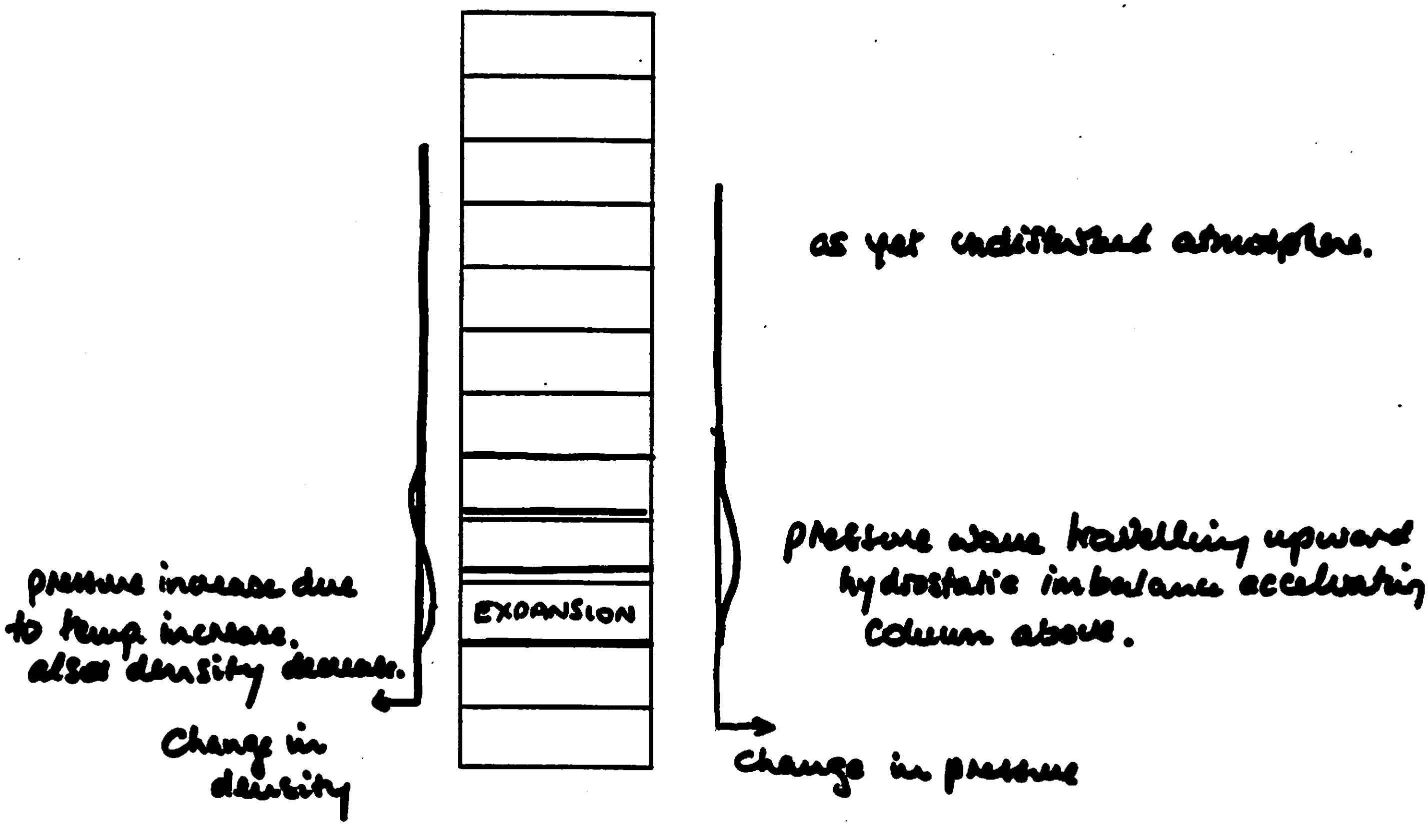

SINGLE ATMOSPHERIC COLUMN

FAST EXPANSION

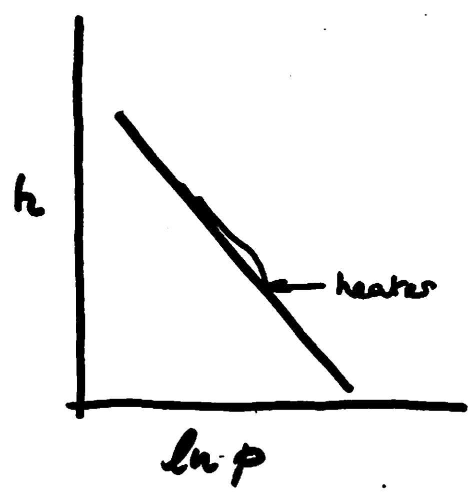

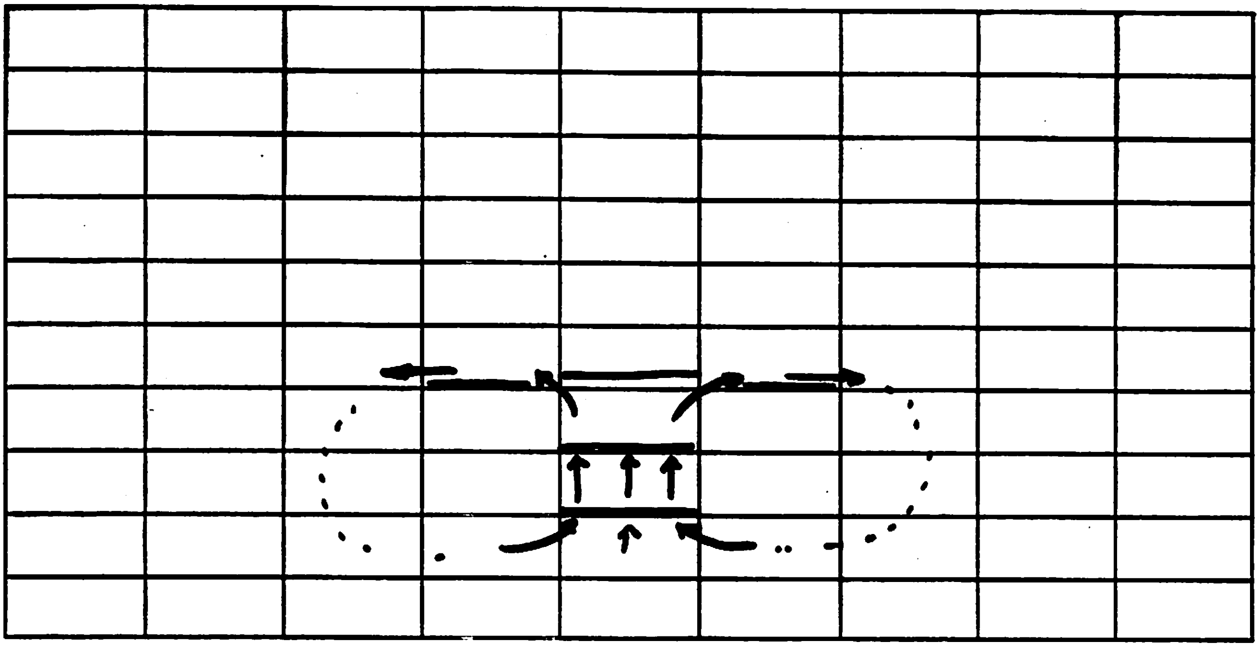

2-D ATMOSPHERE.

THIN HEATER: inflow from adjacent columns
upward jet
adiabatic cooling
outflow to adjacent columns
completion of "twin cell" circulation

Vertical extent of upward flow severely restricted by rapid expansion outside heated region.

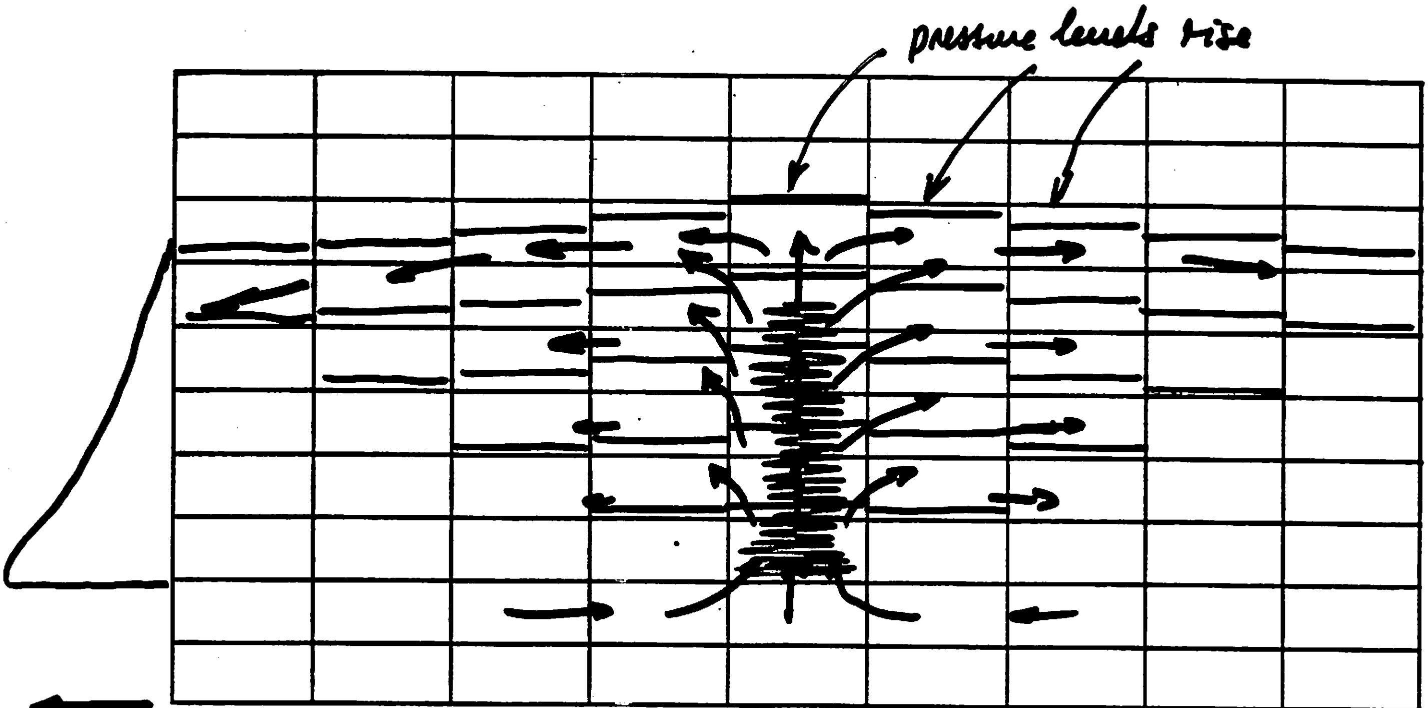

2-D ATMOSPHERE

HEATER WITH EQUAL RATE PER PARTICLE
OVER SEVERAL SCALE HEIGHTS

- inflow from adjacent columns
- strong upward jet
- adiabatic cooling balanced by continued heating
- outflow to adjacent columns — divergence in horizontal flow
- extensive "twin-cell" circulation.
- central atmospheric column rises mainly due to thermal input
- outer columns rise by advected heat but restricted by divergent flow.

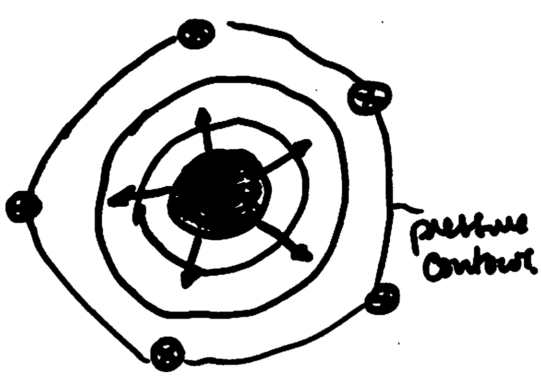

PLAN VIEW.

WHEN THE WIND BLOWS

- FOR "SMALL" SOURCE (in horizontal extent)
  - central column moves out of heated region
  - heating effect short-lived and may not develop to strong event.

- FOR "LONG" SOURCE
  - if wind perpendicular to source length then "small source case"
  - if wind parallel to source length then heating continues for a longer time
    - condition for a large heating event.

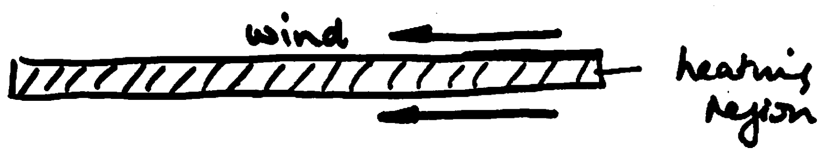

PLAN VIEW

JOULE HEATING SOURCE

Find frictional energy deposited in a vertical column of unit cross section when $|\vec{V}-\vec{u}| = V$

Assume effective thickness of the current layer = 1 scale height.

Then $\quad Q = nH\left(\frac{m}{2}\right)\nu_{ni}V^2$

Writing $\nu_{ni} = K_{ni}N_i$, using Dalgarno's $K_{ni} = 6.3\times10^{-16}\left(\frac{T}{1000}\right)^{0.4}$ $m^3 s^{-1}$

for $T = 1000K$, & $N_i = 10^{11} m^{-3}$

$$\nu_{ni} = 6.3\times10^{-16}\times10^{11} = 6.3\times10^{-5}\,Hz$$

for $V = 1 km\,s^{-1}$ & $H = 10$ km (120 km)

$$Q = 10^{17}\times 5\times10^4\times(16\times1.7\times10^{-27})\times 6.3\times10^{-5}\times10^6$$

$$= 2.0\,mW\,m^{-2}$$

If flow is channelled ($N_i = 2\times10^{12}\,m^{-3}$) then $Q = 40\,mW\,m^{-2}$

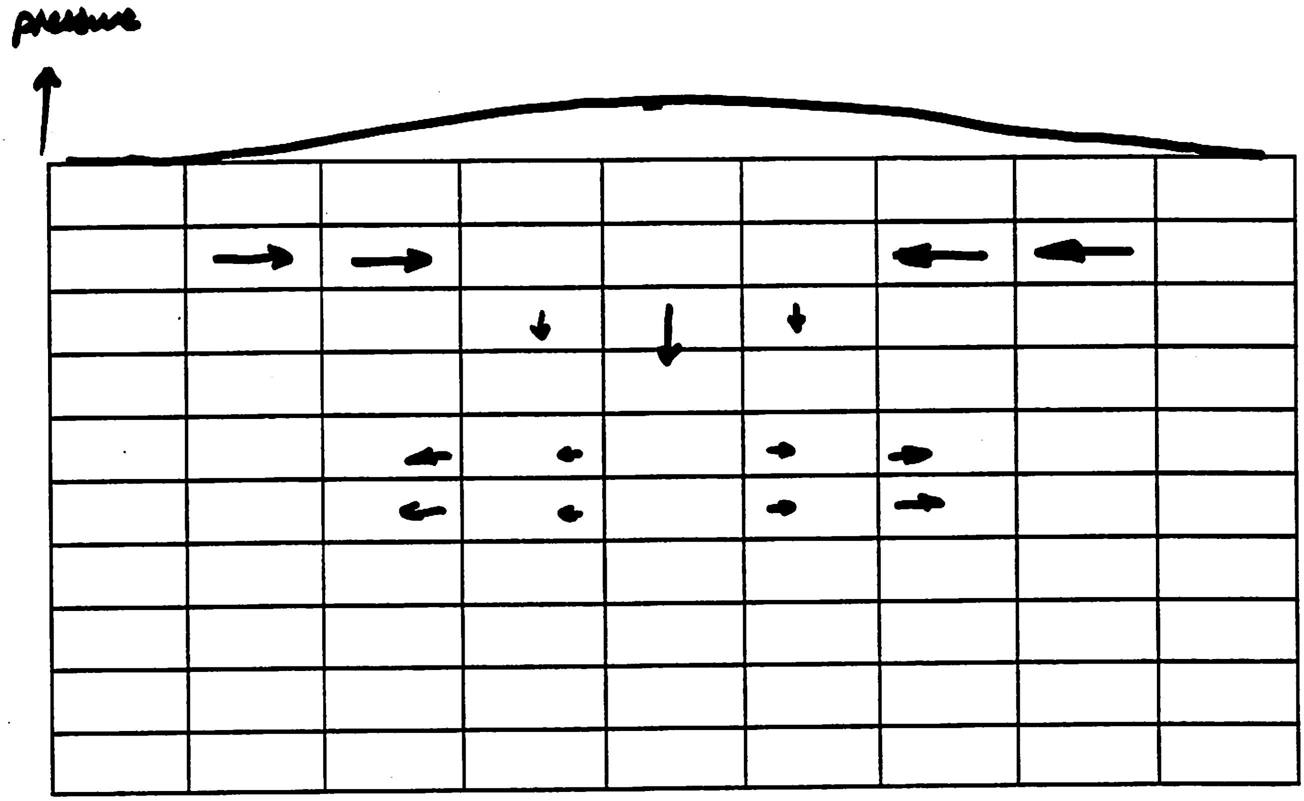

2-D ATMOSPHERE

- WIND-DRIVEN accumulation of mass occurs due to divergent flow
- PRESSURE LEVELS rise initially, but then fall since temperature too low to maintain hydrostatic balance
- AIR PARCELS fall, heating adiabatically
- RISING HORIZONTAL gradients in pressure cause outflow at lower level

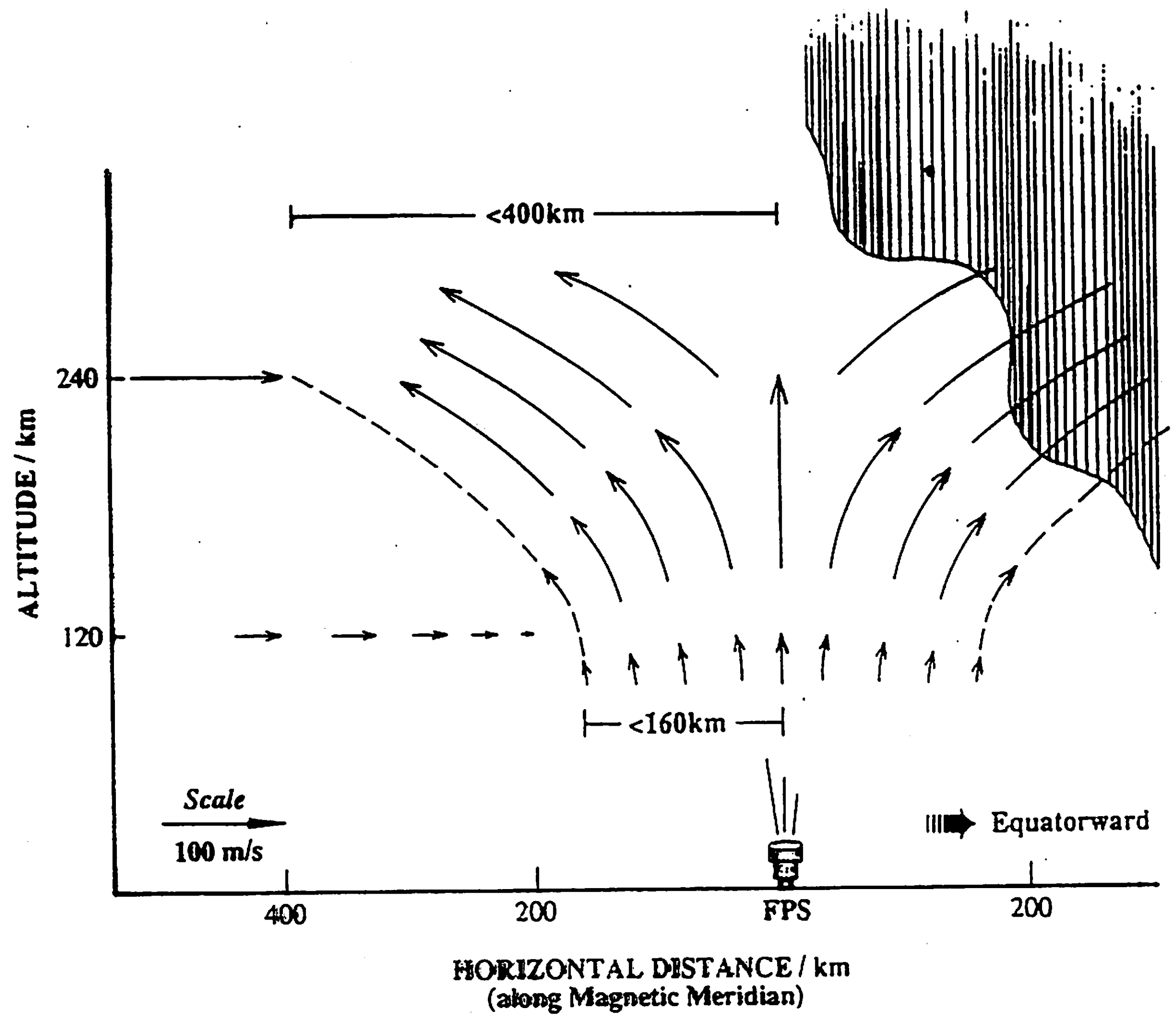

Fig. 5. Schematic model showing the location of the FPS at Poker Flat in relation to the auroral oval at the time of the upwelling. Arrows showing meridional and vertical winds are drawn to scale, and dashed lines mark the estimated size of the upwelling region.

Price et al., 1995

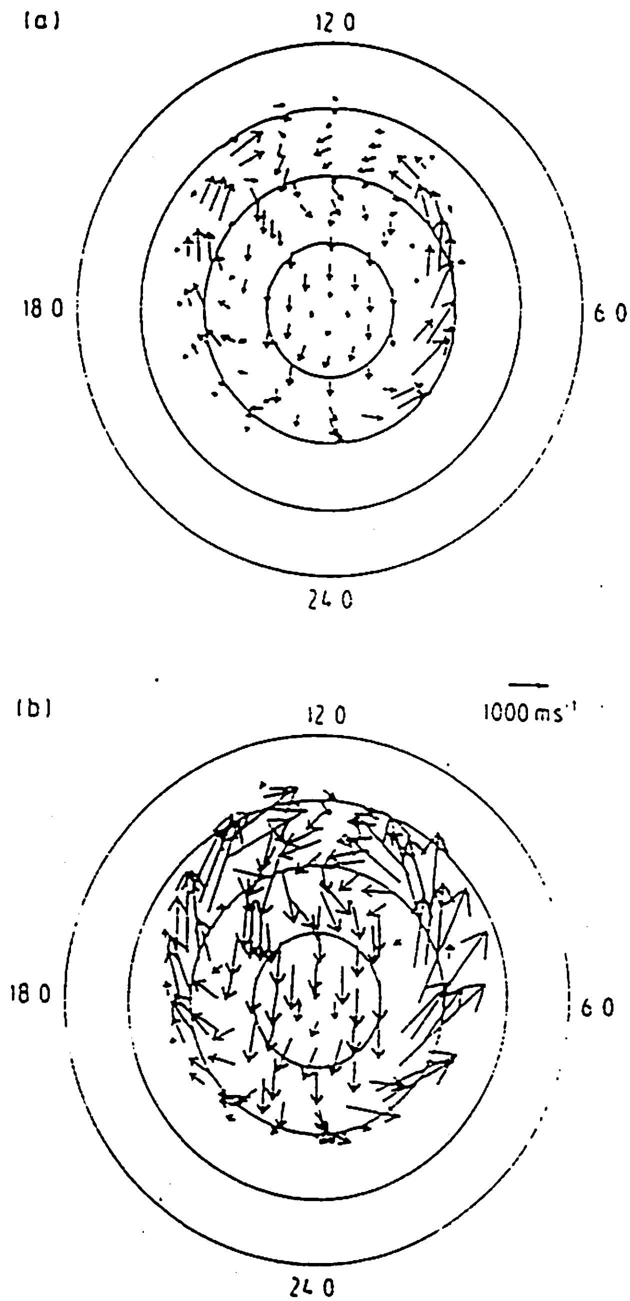

Fig. 1. Polar plots showing ion velocity vectors resulting directly from E × B convection, with E having been taken from the Rice magnetospheric model. a Normal convection; b enhanced convection

Millward et al., 1993

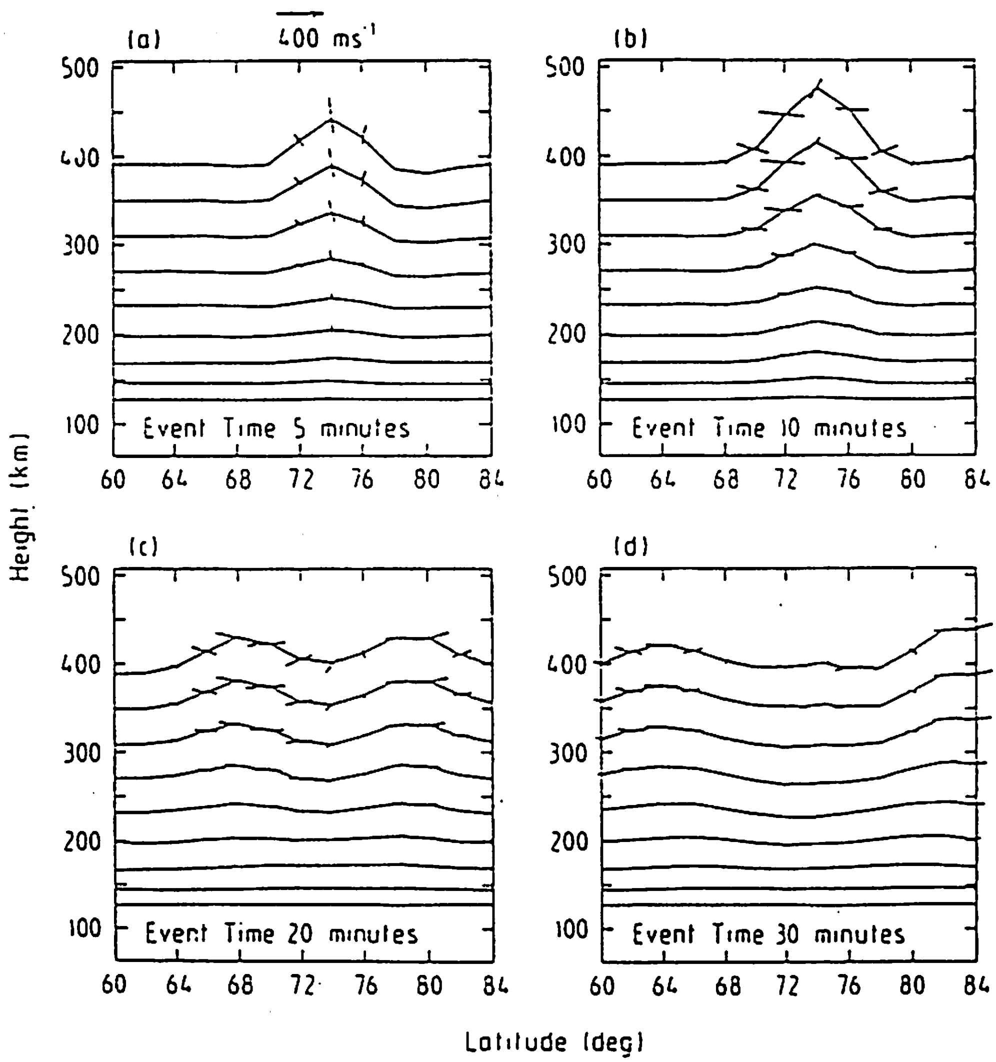

Fig. 4. Heights of neutral air pressure levels 7–15 plotted against latitude for four different event times: a 5 min; b 10 min; c 20 min; and d 30 min. Vectors show the changes in the neutral velocities in the vertical/meridional plane (relative to their initial values, see text). For clarity, vectors representing velocities of less than 50 m s⁻¹ are not shown

Millward et al., 1993

CONCLUSIONS

1. VERTICAL WINDS EXIST WELL ABOVE GLOBAL MEAN VALUES (few m/s) AT ALL LATITUDES, INTERMITTENTLY

2. AT EQUATORIAL, LOW & MIDLATITUDES, EXCURSIONS OF VERTICAL VELOCITIES ~ 10x GLOBAL MEAN ARE FOUND

3. AT HIGH LATITUDES, 100x EXCURSIONS ARE FOUND

4. FOR 100x EXCURSIONS, A MAJOR DISRUPTION (1%) HAS OCCURRED IN THE HYDROSTATIC BALANCE LEADING TO
   - UP/DOWNWELLING
   - RAPID COMPOSITION $\frac{[O]}{[N_2]}$ CHANGES

5. HORIZONTAL SCALE SIZE (~ 400 km on meridian) MAKES THEM SUBGRIDSCALE FOR TIEGCM / CTIM

6. OBSERVED TIMESCALES (HIGH-LAT CASES) CONSISTENT WITH ESTIMATES OF MINIMUM RESPONSE TIMES AT F-REGION HEIGHTS.

7. COMPARATIVE RARITY OF OBSERVATION (HIGH-LAT) EXPLAINED BY a) GEOMETRY OF OBSERVATION

   b) RESTRICTED CONDITIONS IN ATMOSPHERE.